# A MOLECULAR DYNAMICS INVESTIGATION OF HEAT CAPACITY OF NANOGAP CONFINED LIQUID
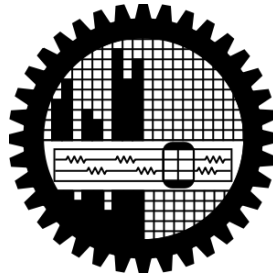
by

**Rifat Mahmud**

**MASTER OF SCIENCE IN MECHANICAL ENGINEERING**
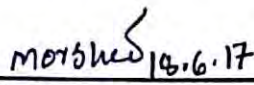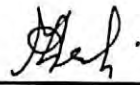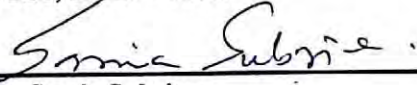


**Department of Mechanical Engineering**

**Bangladesh University of Engineering & Technology**

**June 2017**

The thesis titled **"A Molecular Dynamics Investigation of Heat Capacity of Nanogap Confined Liquid"** submitted by **Rifat Mahmud**, Roll: **1014102013**, Session: **October, 2014**, has been accepted as satisfactory in partial fulfillment of requirement for the degree of **Master of Science in Mechanical Engineering**.

## BOARD OF EXAMINERS

_Morshed 18.6.17_

**Dr. A. K. M. Monjur Morshed**
Associate Professor
Department of Mechanical Engineering
BUET, Dhaka – 1000.

Chairman

(Supervisor)

**Dr. Mohammad Ali**
Professor and Head
Department of Mechanical Engineering
BUET, Dhaka – 1000.

Member

(Ex-Officio)

**Dr. Md. Zahurul Haq**
Professor
Department of Mechanical Engineering
BUET, Dhaka – 1000.

Member

**Dr. Mohammad Nasim Hasan**
Associate Professor
Department of Mechanical Engineering
BUET, Dhaka – 1000.

Member

**Dr. Samia Subrina**
Associate Professor
Department of Electrical and Electronic Engineering
BUET, Dhaka – 1000.

Member

(External)

# CANDIDATE'S DECLERATION

It is hereby declared that this thesis or any part of it has not been submitted elsewhere for the award of any degree or diploma.

June, 2017

Rifat Mahmud

"The journey of a thousand miles begins with a single step"

— Lao Tzu

# ABSTRACT

Geometric confinement with characteristic length comparable to the molecular diameter, can induce a dramatic change in the transport properties of fluids which is of great importance from technological point of view like thermal management of micro/nano electronics, energy conversion devices, micro/nano fluidics devices, energy storage system, drug delivery, understanding different biological systems etc. This study is focused on the fundamental understanding of heat capacity of liquid entrapped in such molecular scale cavity. The study starts by the modeling of heat capacity of bulk liquid. As continuum approximation is not applicable for nanoscale phenomena, molecular dynamics (MD) simulation was used for the modeling. Simplified Lenard Jones (LJ) type molecular model was used in this study.

Heat capacity of the liquid was evaluated from non-equilibrium molecular dynamics (NEMD) simulation following fluctuation formula. Heat capacity of the bulk liquid obtained from the simulation was compared with that of the published literature value and found in excellent agreement. The simulation was extended for the confined liquid by placing the liquid in a nanogap confinement of varying gap thicknesses from 27.8 nm to 0.585 nm. Heat capacity of the confined liquid was observed to vary significantly and the variations follow a very complex relation with the confinement gap thickness. For a limited gap thickness, heat capacity of the nanoconfined liquid was found to be higher than the bulk liquid and beyond that, the nanoconfinement doesn't have any significant effect on the heat capacity of the liquid. Temperature was also found to play a significant role in that complex behavior of the nanoconfined liquid. Heat capacity of the nanoconfined liquid for a certain temperature and gap thickness can be more than double of that of the bulk liquid.

To dissect the underlying facts of this complex behavior, some specific behavioral changes was identified and thoroughly analyzed. It was found that configurational change due to the variation in density, contribution of ballistic and coherent phonon transport, mode of energy transfer, interfacial thermal resistance, modification of vibrational density of states, guided molecular mobility, etc. are some of many underlying key factors that contributes to this anomalous behavior of heat capacity of the nanogap confined liquid.

# TABLE OF CONTENTS

# LIST OF FIGURES

# LIST OF TABLES

# CHAPTER 1
# INTRODUCTION

## 1.1 MOTIVATION FOR THE WORK

Liquid entrapped in molecular scale confinement acts differently than its bulk counterpart [1]. The behavior of liquid entrapped in nanometer length scale confinement is important in a diverse set of technical and scientific contexts. A vast number of technical applications and scientific fields require a prior knowledge on the physics and thermodynamics of such confined fluids. Examples include biological assemblies ranging from multi-subunit protein complexes [1], [2], to membrane topology [3], to RNA packaging [2], where the confined liquid mediates the interactions between chemically, electrostatically, and geometrically complex surfaces. The role of confinement is by no means limited to bio-systems but is also critical in fuel cell technology, where rates of proton transport are controlled by membrane hydration [4]; nanotribology, where the entrapped liquid can control friction between solid surfaces [5]; geosciences, where the organization of confined liquid is essential to the structure and rheology of minerals [6]; and lab-on-a-chip applications, where liquid-flow in confined geometries occurs under the influence of thermal, electrical, mechanical, or substrate chemical patterning driving forces [7]. Particularly in the area of self-assembly, an understanding of the solvent's role is widely recognized as a key element for future materials synthesis [8]. Hence understanding and manipulating fluids at such nanoscale confinement is a matter of growing scientific and technological interests.

Physical dimension plays a key factor in the field of engineering and technology. Simply scaling down the classical equipment/mechanism to micro or nano-scale will not always work as the constituent mechanism; associated parameters and dominance of the parameters vary significantly with the scale. For instances, in classical and micro scale, fluid is treated as a continuum but it does not hold true for the nano-scale. Wave characteristics of energy flow needs to be considered in nano-scale but in classical/micro scale it does not need to be [9]; heat transfer takes place in liquid through the molecular diffusion and molecular interaction, but when the dimension of the liquid is comparable to its mean free path, thermal transportation takes place in ballistic mode

instead of diffusion mode. Thermal conductivity of the nano-gap confined liquid is less than the bulk [10], thin liquid film's molecular mobility is significantly less than the bulk [11], etc.

Nanoconfined fluids exhibit unique structural, dynamic, electro-kinetic and mechanical properties that are different from those of the bulk. For example, depending on the size of the thickness of the entrapped liquid layer, confinement can present a dramatic increase in liquid's viscosity [12]. Experiments and theory have shown that the viscosity of water confined between hydrophilic surfaces increases with confinement, reaching a value of order of magnitude higher than bulk water when confined in a sub-nanometer gap [13]. It is also clear that the usual no-slip boundary condition, that is, zero fluid velocity at the motionless surface, is not universal, and experiments and computer simulations have proved that liquid molecules can slip and have a non-zero velocity at a still solid surface [12]. Furthermore, several studies have indicated that the amount of liquid slip strongly depends on the morphology and chemistry of the stationary solid surface [6]. Some recent studies show that for solid nanocrystals consisting of finite number of atoms, the specific heat capacity varies significantly with the size and temperature of the nanocrystals which is thought to be the contribution of surface free energy to the heat capacity of nanocrystals [14]–[17]. Moreover, the increasing capacity of computer simulation and advanced spectroscopies and microscopies have been continuing to open new vistas and an ever-expanding access to molecular-scale details which provides feasible means to investigate these transport properties of fluids in nanometer-size scale.

All these facts have worked as catalysts to conduct this research work to enrich the traditional understanding on heat capacity of nanogap confined liquids. It is expected that, this work will open up new strategies to investigate the thermal transport properties in complex nanoconfinement systems, such as proteins and cytoskeletal filaments.

## 1.2 OBJECTIVES

The objectives of this research can be enumerated as follows:

1. To develop a molecular model that represents the atomic structure of a two-phase molecular system involving a liquid placed in between two solid surfaces separated by a finite distance and maintaining a predefined temperature. The model will be validated by establishing thermal equilibrium of the molecular system and by monitoring the various thermodynamic and transport properties (e.g. temperature, pressure, density, total energy of the system etc.).

2. To determine the heat capacity of the bulk liquid for different temperatures (below its critical point) and compare these with the bulk liquid data available from existing literatures to validate the applicability of the technique and to extend it for the nanogap confined liquid.

3. To figure out the effect of nanoconfinement on heat capacity of the nanogap confined liquid (from a few nanometers, comparable to phonon mean free path to a sufficiently large value where the effect of nanoconfinement nearly vanishes.)

4. To figure out the effect of variation of temperature on heat capacity of the nanogap confined liquid up-to the critical point of the liquid and compare it with that of the bulk liquid data available from existing literatures.

5. To figure out the combined effect of variation of gap thickness and temperature on heat capacity of the nanogap confined liquid and express it through a mathematical relation.

6. To address some possible reasons that make these behavioral differences of nanoconfined liquid from the bulk ones.

## 1.3 LAYOUT OF THE THESIS

The study presented in this dissertation has addressed the heat capacity of nanogap confined liquid for different gap thicknesses and temperatures. The dissertation has been organized as follows:

In chapter 2, a detail literature review has been presented for a better conception in previous studies regarding the heat capacity of liquids and molecular dynamics simulation that was carried out to

investigate the thermal transport behavior of nanoconfined liquid by different researchers across the globe.

In chapter 3, an overview of the molecular dynamics simulation is presented with the specific scopes and algorithms.

In chapter 4, modelling and formulation of the simulation with detail procedures of coding that has been employed during this research work has been outlined.

In chapter 5, the effect of gap thickness on heat capacity has been investigated with possible explanation of the anomalous behavior of nanoconfined liquid.

In chapter 6, investigation of the effect of temperature on heat capacity of the nanoconfined liquid has been carried out identifying the possible causes of the behavioral difference of nanoconfined liquid.

In chapter 7, the combined effect of gap thickness and temperature on heat capacity is presented with particular focus on maximum heat capacity.

Finally, conclusions and recommendation for future work is discussed in chapter 8 and chapter 9 consecutively.

# CHAPTER 2

# LITERATURE REVIEW

## 2.1 INTRODUCTION

Recent advancement in synthesis, processing, and microanalysis are enabling the routine production of well-characterized materials with structure that varies on the length scale of several nanometers. Examples include microelectronic and optoelectronic devices, microelectromechanical sensors, semiconductor quantum dots and superlattices, polymer nanocomposites, multilayer coatings, etc. Many of these nanoscale structures already have important commercial applications, while others are studied scientifically. Thermal management related to heat storage and effective dissipations are of crucial facts for these devices.

This chapter begins with the present understanding of heat capacity of a substance particularly of liquid under physical confinement. As the size of the domain under consideration begins to approach to molecular level, experimental difficulties arise with the severely limited capabilities for measuring thermal transport in such increasingly small systems. A recent review summarizes the experimental techniques that are being used to probe thermal transport properties at a submicron level [33]. Currently, the only method with nanometer-scale spatial resolution that may be applied to nanometer structures is based on the atomic force microscope (AFM). However, AFM measurements are only beginning to provide an understanding of thermal transport in nanoscale structures; the experimental field is certainly in its infancy. The theory and simulation of nanoscale thermal transport is also at a similarly immature stage. Each still requires further methodological development and the first systematic applications of these methods to heat transport issues are still being refined.

## 2.2 HEAT CAPACITY-THEORETICAL BACKGROUND

In the early modern period, heat was thought to be a measurement of an invisible fluid, known as the caloric [18]. Bodies were capable of holding a certain amount of this fluid, hence the term heat

capacity, named and first investigated by Scottish chemist Joseph Black in the 1750s [19]. Since the development of thermodynamics in the 18th and 19th centuries, scientists have abandoned the idea of a physical caloric, and instead understand heat as a manifestation of a system's internal energy [19].

In 1819, a thermodynamic rule regarding heat capacity of crystalline solid phase were proposed by French physicists Pierre Louis Dulong and Alexis Thérèse Petit, later known to be the famous Dulong–Petit law [20]. They found experimentally that for many solids at room temperature, $C_v \approx 3R = 25$ JK$^{-1}$mol$^{-1}$ which is consistent with equipartition theory: energy added to solids takes the form of atomic vibrations and both kinetic and potential energy is associated with the three degrees of freedom of each atom. Although heat capacity for many elements at room temperature are indeed close to 3R, low-temperature measurements found a strong temperature dependence of heat capacity [20]. Actually, heat capacity tends to be zero as temperature approaches to 0 K.

The low-temperature behavior can be explained by quantum theory. The first explanation was proposed by Einstein in 1906 [20]. He considered a solid as an ensemble of independent quantum harmonic oscillators vibrating at a constant frequency. For a quantum harmonic oscillator the Einstein-Bose statistics must be applied (rather than Maxwell-Boltzmann statistics and equipartition of energy for classical oscillators) and the statistical distribution of energy in the vibrational states gives average energy [18]. The Einstein formula gives a temperature dependent heat capacity that approaches 3R as temperature tends to be infinity and approaching 0 as temperature tends to absolute zero. It can be showed that Einstein's formula approaches Dulong – Petit law at high temperature. Although the general match of the data obtained from Einstein's model with experimental ones is reasonable, it is not exact. Einstein formula predicts faster decrease of heat capacity as compared with the experimental data [20].

Large exceptions at the lower end involve solids composed of relatively low-mass, tightly bonded atoms, such as beryllium at 2.0 R, and diamond at only 0.735 R [18]. The latter conditions create larger quantum vibrational energy spacing, thus many vibrational modes have energies too high to be populated (and thus are "frozen out") at room temperature. At the higher end of possible heat capacities, heat capacity may exceed 3R by modest amounts, due to contributions from an-

harmonic vibrations in solids, and sometimes a modest contribution from conduction electrons in metals. These are not degrees of freedom treated in the Einstein or Debye theories.

Einstein's oscillator treatment of specific heat gave qualitative agreement with experiment and gave the correct high temperature limit (the Law of Dulong and Petit). The quantitative fit to experiment was improved by Debye's recognition that there was a maximum number of modes of vibration in a solid [20]. He pictured the vibrations as standing wave modes in the crystal, similar to the electromagnetic modes in a cavity which successfully explained blackbody radiation. The density of states for these modes, which are called "phonons", is of the same form as the photon density of states in a cavity. Debye advanced the Einstein's model by treating the quantum oscillators as collective modes in the solid phonons.

The Debye model correctly predicts the low temperature dependence of the heat capacity. And just like the Einstein model, it also recovers the Dulong–Petit law at high temperatures but due to simplifying assumptions, its accuracy suffers at intermediate temperatures [18].

The Einstein-Debye phonon model produce agreement with the low-temperature cubic dependence of specific heat upon temperature. Explaining the drastic departure from the Law of Dulong and Petit was a major contribution of the Einstein and Debye models. The final step in explaining the low temperature specific heat of metals was the inclusion of the electron contribution to specific heat. For instance, the existing data show that the Debye phonon model with its cubic dependence on temperature matches the silicon data to very low temperatures. But the copper shows a departure from the cubic dependence, showing evidence of electron specific heat [21].

Avramov and Michailov [14] extends the Einstein model for heat capacity of solids to nanoclusters. In the case of small phases, the contribution of surface energy to overall thermodynamic properties of the system is essential [14]. On that physical background, the heat capacity depends on the size of cluster through its interface energy. Employing the same relation between Einstein temperature and the cluster melting point as that for the infinitely large phase, they derived a simple expression for the heat capacity, $C_V(n)$, dependence on the number of atoms in the cluster, n. They explained the experimentally observed increase of $C_V(n)$ compared to $C_V$ ($\infty$) of an infinitely large homogeneous phase, with lowering of the Einstein temperature due to

the contribution of the cluster interface energy. The heat capacity in the model presents good results at high temperature analogous to the classical Dulong and Petit 3R limit and tends to fall to zero for temperature approaching as required by the third law of thermodynamics. The model reported could be applied to various systems with nanoparticles, where the knowledge of specific heat is important; for example- formation of nanocomposite materials, the initial stages of formation of fogs, smog and clouds, etc.

A general theory of the heat capacity of liquids has not yet been achieved [18], and is still an active area of research. It was long thought that phonon theory is not able to explain the heat capacity of liquids, since liquids only sustain longitudinal, but not transverse phonons, which in solids are responsible for 2/3 of the heat capacity. However, Brillouin scattering experiments with neutrons and with X-rays, confirming an intuition of Yakov Frenkel, [22] have shown that transverse phonons do exist in liquids, albeit restricted to frequencies above a threshold called the Frenkel frequency. Since most energy is contained in these high-frequency modes, a simple modification of the Debye model is sufficient to yield a good approximation to experimental heat capacities of simple liquids [23].

Amorphous materials can be considered as a type of liquid. The specific heat of amorphous materials has characteristic discontinuities at the glass transition temperature. These discontinuities are frequently used to detect the glass transition temperature where a supercooled liquid transforms to a glass [23].

Although a simple modification of traditional theories of heat capacity of solids can explain and predict heat capacity of bulk liquids with great accuracy, this continuum approach fails vigorously to predict the heat capacity of nanogap confined liquid theoretically. This leads to imply computational approaches to predict heat capacity of such systems.

The behavioral difference of heat capacity of the confined liquid from its bulk counterparts lies in its modes of phonon transport. When the dimensionality of the system is large enough compared to the mean free path of phonon, phonon transmission is diffusive [23]–[26] . But when the system size shrinks to a scale that is comparable to the mean free path of phonon at that specified state, phonon transmission is no more diffusive, it is either ballistic or coherent or transient between diffusive and ballistic as studied by many earlier researchers [24], [28]. The figure shown below presents the length dependent phonon transportation for hollow silicon [24].
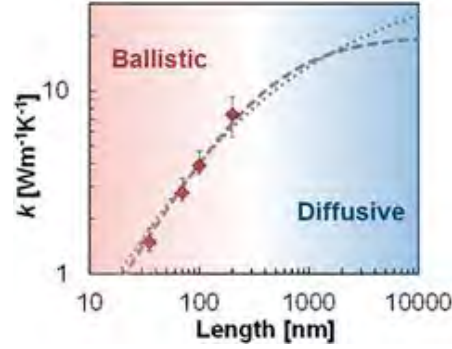
Figure 1: Phonon transport for different system lengths (For holey Si) [24]

For other materials like carbon nanotubes (CNT), as the dimension extends from nanometer to millimeter, phonon transmission shifted to diffusive regime from ballistic ones [29]. Yamamoto et. al. [29] presented a theoretical scheme that seamlessly handled the crossover from fully ballistic to diffusive thermal transport regimes and applied it to carbon nanotubes. At room temperature, the micrometer-length nanotubes belonged to the intermediate regime in which ballistic and diffusive phonons coexist. The length dependences of thermal conductivity revealed the variation of the balance between ballistic and diffusive heat conduction [29].
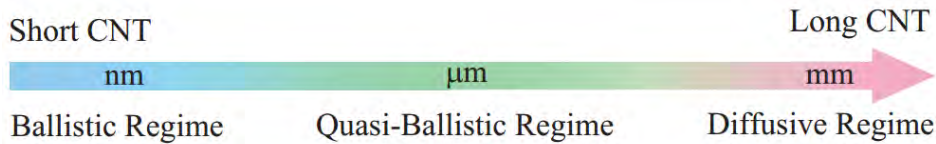


Figure 2: Length dependent phonon transport in CNT [29].

Hence the first step of analyzing phonon transmission mechanism through a medium is to determine its mean free path at that medium for that specified conditions. For liquid Ar, mean free path at the system specified state has been calculated using equation (24) as stated earlier.

As a very preliminary knowledge on phonon transportation mechanism, it is well known that diffusive transmission occurs when phonon transmission is impeded by scattering phenomenon like phonon-phonon scattering, boundary scattering, scattering due to impurities and imperfections etc [28]. But when the system size shrinks to nanoscale, lesser than the mean free path of phonon, it is expected that no collision would take place rendering classical collision based theory useless [28]. In this case phonon transport is said to be ballistic [28]. In this mode of phonon transport, the

phonon alters its motion only upon collision with the walls. In the case of a wire suspended in air/vacuum, the surface of the wire plays the role of the box reflecting the phonons and preventing them from exiting towards the empty space/open air [30]. Actually, ballistic conduction is the unimpeded flow of charge, or energy-carrying particles, over relatively long distances in a material. Normally, transport of phonon is dominated by scattering events, which relax the carrier momentum in an effort to bring the conducting material to equilibrium [28]. Ballistic conduction is typically observed in quasi-1D structures, such as carbon nanotubes or silicon nanowires, because of extreme size quantization effects in these materials. Ballistic conduction is not limited to phonons but can also apply to electrons (or holes) [28].
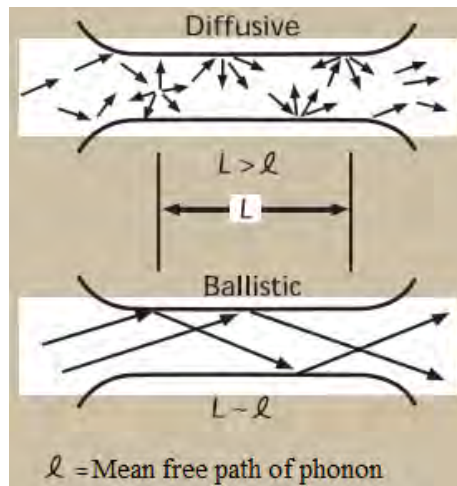


Figure 3: Diffusive and Ballistic transport of phonons in a one-dimensional wire [30]

In the cases of such small dimensionality, phonon density of states, commonly known as vibrational density of states (VDOS) of phonon is greatly modified as stated by some earlier researchers. Modification in VDOS significantly modify phonon transportation which in turns modify its thermal energy transportation and retaining capability [17], [31]. These works show that for ballistic transmission, in general, phonon transmission occurs in higher frequency modes up-to a critical value [17]. This critical value is the system dimensionality when the vibrational modes of the system are restrained due to its transition from liquid to solid state. That is, when the system consists of nearly one restrained monoatomic layer [17].

## 2.3 COMPUTATIONAL ANALYSIS OF TRANSPORT PROPERTIES AT NANOSCALE

Recent advances in computer power and simulation have opened up new horizon in computational analysis of transport properties at nanometer size-scales. These techniques enable to predict and evaluate thermodynamic and material properties of substances in great accuracy and reliability where neither experimental nor direct analytical data are readily available. Understanding and manipulating fluids at the nanoscale is a matter of growing scientific and technological interest. Different aspects of materials in sub-micron level have been revealed through molecular dynamics simulations. Previously several molecular dynamics simulations have been employed to show that the viscous shear forces in nanoconfined water can be orders of magnitudes larger than in bulk water if the confining surfaces are hydrophilic, whereas they greatly decrease when the surfaces are increasingly hydrophobic [13]. This decrease of viscous forces is quantitatively explained with a simple model that includes the slip velocity at the water surface interface. Comparison of the experimental data with the model shows that interfacial viscous forces and compressive dissipation in nanoconfined water can decrease up to two orders of magnitude due to slippage. These results offer a new understanding of interfacial fluids, which can be used to control flow at the nanoscale [13].

The thermal conductivity of nanofluids was computed using different methods for various volume fractions of nanoparticle loadings earlier [8], [9]. These showed the ability of molecular dynamics to predict the enhanced thermal conductivity of nanofluids. The results showed that the thermal transport enhancement of nanofluids is mostly due to the increased movement of liquid atoms in the presence of nanoparticle. Diffusion coefficients was also calculated for base fluid and nanofluids. Similarity of enhancement in thermal conductivity and diffusion coefficient for nanofluids indicated similar transport process for mass and heat [32]. With Molecular dynamics simulations, Li et.al. [33] have shown that, for wires of nanometer diameter, the thermal conductivities could be two orders of magnitude smaller than that of bulk silicon [33].

Cheng Shao and Hua Bao [34], using molecular dynamics simulations, systematically investigate the net thermal resistance of two interfaces and the confined thin film, and compare the results with the predictions from the thermal circuit model [34]. The results indicate that when the thickness of a disordered thin film is greater than 2 nm, the net resistance across the film is almost linearly dependent on the film thickness and always larger than the prediction of the thermal circuit

model. For extremely small thickness (<2 nm), the amorphous thin film has similar resistance to the crystalline counterpart. The existence of alloy region between two dissimilar materials could reduce the interfacial resistance when the alloy thickness is a few atomic layers, but would enhance the resistance when the alloy thickness is larger [34].

Non-equilibrium classical molecular dynamics simulation was carried out by Morshed et.al. to study the temperature dependence of thermal transport across nanogap confined liquid [35]. The research was focused on the temperature response behavior of nanoconfined liquid subjected to different temperature environment. It was found that the molecular mobility and thermal conductance of liquid reduces significantly due to the confinement in a nanometer scale cavity. The simulation also reveals that thermal resistance responses oppositely to the change in temperature for the nanoconfined liquid compared to the bulk ones; thermal resistance of the nanoconfined liquid was observed to decrease with the increase of temperature whereas it increases for the bulk liquid. Thermal resistance of the confined liquid and its dependence on temperature was also observed to strongly depend on the gap thickness [35].

Detailed dynamic, thermodynamic and pseudo-thermodynamic behaviors were reported for the glass transition in confined geometries for both small molecules confined in nanopores and for ultrathin polymer films by some earlier researchers [2]. Molecular dynamics simulations have also revealed the molecular-level mechanisms for experimental observations like Entropy-driven structure and dynamics in carbon nano-crystallites [36]. The magnitude of out-of-plane ripples, binding energy between layers, and frequency of characteristic planar modes have been reported over a range of nano-crystallite sizes and temperatures [36].

The case of nanofluids is a good illustration of the role that can be played by molecular simulation in the interpretation of complex situations. Although many interpretations have been proposed to explain the reported experimental results, it is only simulation of simple models that has been able to disprove some of these interpretations and to demonstrate the validity of the alternative, aggregation scenario. Interestingly, the use of complex models with accurate interaction force fields is not, in general, needed to answer the basic qualitative questions raised by such experimental approaches [37].

Rajabpour et al. investigated the specific heat capacity of water-Cu nanofluids through molecular dynamics simulation. The obtained results show that the specific heat capacity of Cu-water nanofluids decreases gradually with increasing volume concentration of nanoparticles. The simulation results are compared with two existing applied models for the prediction of the specific heat of the nanofluid. The obtained specific heat results from the MD simulation and the prediction from the thermal equilibrium model for calculating specific heat of nanofluids exhibit good agreement and the other simple mixing model fails to predict the specific heat capacity of Cu-water nanofluids particularly at high volume fractions.

Classical molecular dynamics simulations were performed to study structural and dynamic properties of water confined within graphite surfaces separated by a distance varying between 7 and 14.5 Å, at a constant water density of 1 g/cm$^3$ [38]. Results at 298 K showed the formation of a well-ordered structure constituted by water-layers parallel to the graphite surfaces. The water molecules in layers in contact with the surface had a tendency to orient their dipole parallel to the surface. Such ice-like structure may have, however, different structural and dynamical properties than those of ice.

Hirunsuit and Balbuena [39] estimated the heat capacity of uranium mononitride (UN) by molecular dynamics (MD) calculation with the Morse-type potential function added to the Busing–Ida type potential in the temperature range 300–2500 K [39]. The parameters of the interatomic potential were determined by fitting the changes in the lattice parameters with temperature and pressure to those in the literatures. The thermal expansion coefficient and the compressibility were calculated. The heat capacity at constant volume ($C_V$) was evaluated from the variation of the internal energy of the system by the fixed volume MD calculation [39].

Thus, it is evident that atomic simulations are providing new data and exciting insights into various manufacturing processes and tribological phenomenon that cannot be obtained readily in any other way—theory, or experiment. Hence with proper modelling and validation, computational analysis of transport properties can be a great resource to meet the quest for knowledge in nanometer size-scales.

## 2.4  CONCLUSIONS

The existing literatures show that although there are straight-forward analytical methods to determine the heat capacity of solid, a direct formulation dedicated to determine the heat capacity of liquid is still in infantry though a simple modification of these formulation provide reasonably good prediction of heat capacity of liquids. Moreover, these models can be extended for solid nanoclusters or nanocrystals consisting of finite number of atoms. Previous studies reveal that heat capacity of such nanoclusters or nanocrystals depends on both the number of atoms i.e. size and temperature of the solid. But no such models have been incorporated for liquids in nanoscale investigations. Molecular dynamics simulations, among many other computational methods, have broaden the opportunity to investigate transport properties of such systems where neither theoretical nor experimental method can be incorporated. The direct application of molecular dynamics method in such problems have been justified by many earlier researchers.

# CHAPTER 3
# SIMULATION METHODOLOGY

## 3.1 INTRODUCTION

Computer simulations reproduce the behavior of a system using a mathematical model. The model is then validated by its ability to describe the system behavior in a few selected cases, simple enough to allow a solution to be computed from the equations. Computer simulations have become a useful tool for the mathematical modeling of many natural systems in physics (computational physics), astrophysics, climatology, chemistry and biology, human systems in economics, psychology, social science, and engineering. Accurate computer models can provide information that is very difficult to obtain directly with experiments. The accuracy of these simulations depends on the quality of the "force field" that emulates the underlying physics. These force fields describe how the energy of the molecule responds to various events needed for function. In many cases, they imply a considerable amount of simplification in order to eliminate all the complexities invariably associated with real world problems, and make the problem solvable.

## 3.2 MOLECULAR DYNAMICS VS MONTE CARLO SIMULATION

Molecular dynamics (MD) is a computer simulation technique where the time evolution of a set of interacting atoms is followed by integrating their equations of motion.

In molecular dynamics, the laws of classical mechanics, and most notably Newton's law are followed:

$$F_i = m_i a_i \tag{1}$$

for each atom 'i' in a system constituted by 'N' atoms. Here, 'm$_i$' is the atom mass, '$a_i = \frac{d^2 r_i}{dt^2}$' its acceleration, and 'F$_i$' the force acting upon it, due to the interactions with other atoms. Therefore, in contrast with the Monte Carlo method, molecular dynamics is a deterministic technique: given an initial set of positions and velocities, the subsequent time evolution is in

principle completely determined. In more pictorial terms, atoms will "move" into the computer, bumping into each other, wandering around, oscillating in waves along with their neighbors, perhaps evaporating away from the system if there is a free surface, and so on, in a way pretty similar to what atoms in a real substance would do.

The computer calculates a trajectory in a 6N-dimensional phase space (3N positions and 3N momenta). However, such trajectory is usually not particularly relevant by itself. Molecular dynamics is a statistical mechanics method. Like Monte Carlo, it is a way to obtain a set of configurations distributed according to some statistical distribution function, or statistical ensemble. An example is the microcanonical ensemble, corresponding to a probability density in phase space where the total energy is a constant :

$$\delta(H(\Gamma) - E) \tag{2}$$

Here, 'H($\Gamma$)' is the Hamiltonian, and '$\Gamma$' represents the set of positions and momenta '$\delta$' is the Dirac function, selecting out only those states which have a specific energy 'E'. Another example is the canonical ensemble, where the temperature 'T' is constant and the probability density is the Boltzmann function

$$exp\left(-H(\Gamma)\big/_{\kappa_B T}\right) \tag{3}$$

According to statistical physics, physical quantities are represented by averages over configurations distributed according to a certain statistical ensemble. A trajectory obtained by molecular dynamics provides such a set of configurations. Therefore, a measurement of a physical quantity by simulation is simply obtained as an arithmetic average of the various instantaneous values assumed by that quantity during the MD run.

Statistical physics and statistical thermodynamics are the link between the microscopic behavior and thermodynamics. In the limit of very long simulation times, one could expect the phase space to be fully sampled, and in that limit this averaging process would yield the thermodynamic properties. In practice, the runs are always of finite length, and one should exert caution to estimate when the sampling may be good ("system at equilibrium") or not. In this way, MD simulations can be used to measure thermodynamic properties and therefore evaluate, say, the phase diagram of a specific material.

Beyond this "traditional" use, MD is also used for other purposes, such as studies of non-equilibrium processes and as an efficient tool for optimization of structures overcoming local energy minima (simulated annealing).

## 3.3 LIMITATION OF MD SIMULATIONS

Molecular dynamics is a very powerful technique but has limitations. The most important of them are quickly examined below.

### 3.3.1 Use of Classical Forces

One could immediately ask: how can we use Newton's law to move atoms, when everybody knows that systems at the atomistic level obey quantum laws rather than classical laws, and that Schrödinger's equation is the one to be followed?

A simple test of the validity of the classical approximation is based on the de Broglie thermal wavelength [64], defined as:

$$\Lambda = \sqrt{\frac{2\pi\hbar^2}{M\kappa_B T}} \tag{4}$$

where M is the atomic mass and T the temperature. The classical approximation is justified if $\Lambda \ll a$, where a is the mean nearest neighbor separation. If one considers for instance liquids at the triple point, $\Lambda/a$ is of the order of 0.1 for light elements such as Li and Ar, decreasing further for heavier elements. The classical approximation is poor for very light systems such as $H_2$, He, Ne.

Moreover, quantum effects become important in any system when T is sufficiently low. The drop in the specific heat of crystals below the Debye temperature[65], or the anomalous behavior of the thermal expansion coefficient are well known examples of measurable quantum effects in solids.

Molecular dynamics results should be interpreted with caution in these regions.

### 3.3.2 Realism of forces

In molecular dynamics, atoms interact with each other. These interactions originate forces which act upon atoms, and atoms move under the action of these instantaneous forces. As the atoms move, their relative positions change and forces change as well.

The essential ingredient containing the physics is therefore constituted by the forces. A simulation is realistic – that is, it mimics the behavior of the real system – only to the extent that interatomic forces are similar to those that real atoms (or, more exactly, nuclei) would experience when arranged in the same configuration.

In molecular dynamics simulation, forces are usually obtained as the gradient of a potential energy function, depending on the positions of the particles. The realism of the simulation therefore depends on the ability of the potential chosen to reproduce the behavior of the material under the conditions at which the simulation is run.

### 3.3.3 Time and Size Limitation

Typical MD simulations can be performed on systems containing thousands – or, perhaps, millions of atoms and for simulation times ranging from a few picoseconds to hundreds of nanoseconds. While these numbers are certainly respectable, it may happen to run into conditions where time and/or size limitations become important.

A simulation is "safe" from the point of view of its duration when the simulation time is much longer than the relaxation time of the quantities we are interested in. However, different properties have different relaxation times. In particular, systems tend to become slow and sluggish in the proximity of phase transitions and it is not uncommon to find cases where the relaxation time of a physical property is orders of magnitude larger than times achievable by simulation.

A limited system size can also constitute a problem. In this case one has to compare the size of the MD cell with the correlation lengths of the spatial correlation functions of interest. Again, correlation lengths may increase or even diverge in proximity of phase transitions and the results are no longer reliable when they become comparable with the box length.

## 3.4 MODELING THE PHYSICAL SYSTEM

The main ingredient of a simulation is a model for the physical system. For a molecular dynamics simulation, this amounts to choosing the potential: a function V ($r_1$, ………$r_N$) of the positions of the nuclei, representing the potential energy of the system when the atoms are arranged in that specific configuration. This function is translationally and rotationally invariant, and is usually constructed from the relative positions of the atoms with respect to each other, rather than from the absolute positions.

Forces are then derived as the gradients of the potential with respect to atomic displacements:

$$F_i = -\nabla_{r_i} V(r_1, \dots\dots\dots, r_N) \tag{5}$$

This form implies the presence of a conservation law of the total energy E = K + V, where K is the instantaneous kinetic energy.

The simplest choice for V is to write it as a sum of pairwise interactions:

$$V(r_1, \dots\dots\dots, r_N) = \sum_i \sum_{j>i} \emptyset(|r_i - r_j|) \tag{6}$$

The clause j >i in the second summation has the purpose of considering each atom pair only once. In the past, most potentials were constituted by pairwise interactions, but this is no longer the case. It has been recognized that the two-body approximation is very poor for many relevant systems, such as metals and semiconductors. Various kinds of many-body potentials are now of common use in condensed matter simulation.

## 3.5 THE LENNARD-JONES POTENTIAL

The Lennard-Jones 12-6 potential [66] is given by the expression

$$\emptyset(r) = 4\varepsilon \left[ \left(\frac{\sigma}{r}\right)^{12} - \left(\frac{\sigma}{r}\right)^{6} \right] \tag{7}$$

for the interaction potential between a pair of atoms.

This potential has an attractive tail at large r, it reaches a minimum around 1.122σ, and it is strongly repulsive at shorter distance, passing through 0 at r = σ and increasing steeply as r is decreased further.

The term $\sim 1/r^{12}$, dominating at short distance, models the repulsion between atoms when they are brought very close to each other. Its physical origin is related to the Pauli principle: when the electronic clouds surrounding the atoms starts to overlap, the energy of the system increases abruptly. The exponent 12 was chosen exclusively on a practical basis: The Lennard-Jones equation is particularly easy to compute. In fact, on physical grounds an exponential behavior would be more appropriate.

The term $\sim 1/r^{6}$, dominating at large distance, constitute the attractive part. This is the term which gives cohesion to the system. A $1/r^{6}$ attraction is originated by van der waals dispersion forces, originated by dipole-dipole interactions in turn due to actuating dipoles. These are rather weak interactions, which however dominate the bonding character of closed-shell systems, that is, rare gases such as Ar or Kr. Therefore, these are the materials that a LJ potential could mimic fairly well. The parameters ε and σ are chosen to fit the physical properties of the material.

On the other hand, a LJ potential is not at all adequate to model situations with open shells, where strong localized bonds may form (as in covalent systems), or where there is a delocalized "electron sea" where the ions sit (as in metals). In these systems, the two-body interactions scheme itself fails very badly.

However, regardless of how well it is able to model actual materials, the LJ 12-6 potential constitutes nowadays an extremely important model system. There is a vast body of papers who investigated the behavior of atoms interacting via LJ on a variety of different geometries (solids, liquids, surfaces, clusters, two-dimensional systems, etc.). One could say that LJ is the standard potential to use for all the investigations where the focus is on fundamental issues, rather than studying the properties of a specific material. The simulation work done on LJ systems helped us (and still does) to understand basic points in many areas of condensed matter physics, and for this reason the importance of LJ cannot be underestimated.

In practical applications, it is customary to establish a cutoff radius '$r_c$' and disregard the interactions between atoms separated by more than '$r_c$'. This results in simpler programs and

enormous savings of computer resources, because the number of atomic pairs separated by a distance r grows as $r^2$ and becomes quickly huge.

A simple truncation of the potential creates a new problem though: whenever a particle pair "crosses" the cutoff distance, the energy makes a little jump. A large number of these events is likely to spoil energy conservation in a simulation. To avoid this problem, the potential is often shifted in order to vanish at the cutoff radius:

$$V(r) = \begin{cases} \emptyset_{LJ}(r) - \emptyset_{LJ}(r_c) & if\ r\ \le\ R_c \\ 0 & if\ r > R_c \end{cases} \tag{8}$$

Physical quantities are of course affected by the potential truncation. The effects of truncating a full-ranged potential can be approximately estimated by treating the system as a uniform (constant density) continuum beyond 'r$_c$'. For a bulk system (periodic boundary conditions along each direction), this usually amounts to a constant additive correction. For example, the potential tail (attractive) brings a small additional contribution to the cohesive energy, and to the total pressure. Truncation effects are not so easy to estimate for geometries with free surfaces, due to the lower symmetry, and can be rather large for quantities like surface energy.

## 3.6 PERIODIC BOUNDARY CONDITIONS (PBC)

To eliminate the surface effects, periodic boundary condition (PBC) is used in molecular simulation. In PBC, the cubical simulation box is replicated throughout space to form an infinite lattice. In the course of the simulation, when a molecule moves in the central box, its periodic image in every one of the other boxes moves with exactly the same orientation in exactly the same way. Thus, as a molecule leaves the central box, one of its images will enter through the opposite face. There are no walls at the boundary of the central box, and the system has no surface. A three-dimensional version of such a periodic system is shown in Figure 4. As a particle moves through a boundary, all its corresponding images move across their corresponding boundaries. The number of particles in the central box (and hence in the entire system) is conserved.
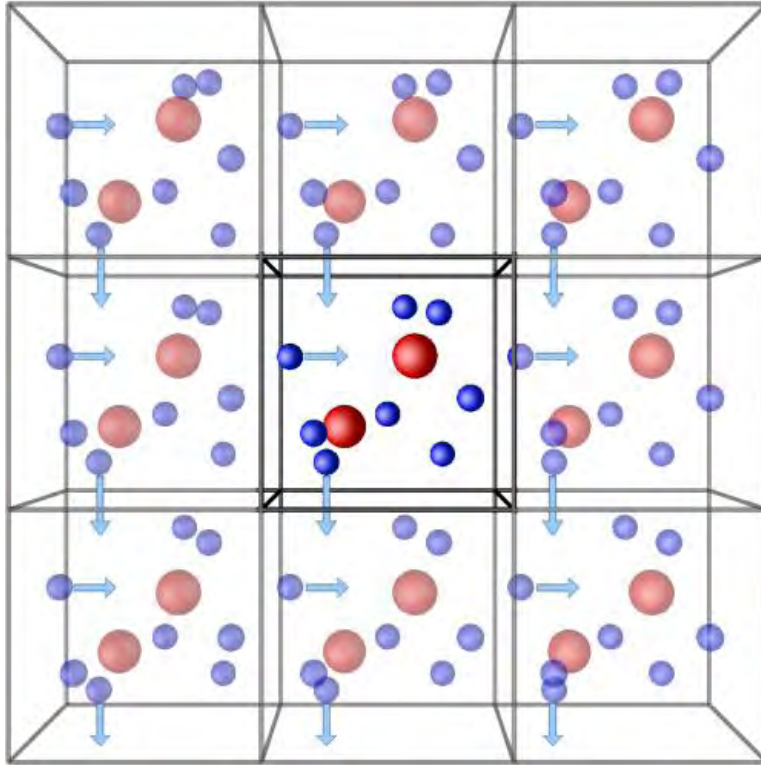
Figure 4: Periodic boundary condition (The central box is outlined with a thicker line)

## 3.7 TIME INTEGRATION ALGORITHM

The engine of a molecular dynamics program is its time integration algorithm, required to integrate the equation of motion of the interacting particles and follow their trajectory.

Time integration algorithms are based on finite difference methods, where time is discretized on a finite grid, the time step $\Delta t$ being the distance between consecutive points on the grid. Knowing the positions and some of their time derivatives at time t (the exact details depend on the type of algorithm), the integration scheme gives the same quantities at a later time t+$\Delta t$. By iterating the procedure, the time evolution of the system can be followed for long times.

Two popular integration methods for MD calculation are the Verlet algorithm and predictor-corrector algorithm. They are quickly presented in the sections below.

### 3.7.1 The Verlet Algorithm

In molecular dynamics, the most commonly used time integration algorithm is probably the so-called Verlet algorithm [67]. The basic idea is to write two third-order Taylor expansions for the positions r(t), one forward and one backward in time. Calling 'v' the velocities, 'a' the accelerations, and 'b' the third derivatives of 'r' with respect to 't', one has:

$$r(t + \Delta t) = r(t) + v(t)\Delta t + (1/2) \ a(t) \ \Delta t^2 + (1/6) \ b(t) \ \Delta t^3 + O(\Delta t^4)$$

$$r(t - \Delta t) = r(t) - v(t)\Delta t + (1/2) \ a(t) \ \Delta t^2 - (1/6) \ b(t) \ \Delta t^3 + O(\Delta t^4) \tag{9}$$

Adding the two expressions gives

$$r(t + \Delta t) = 2r(t) - r(t - \Delta t) + a(t)\Delta t^2 + O(\Delta t^4) \tag{10}$$

This is the basic form of the verlet algorithm. Since we are integrating Newton's equations, a(t) is just the force divided by the mass, and the force is in turn a function of the positions r(t):

$$a(t) = - (1/m)\nabla V(r(t)) \tag{11}$$

As one can immediately see, the truncation error of the algorithm when evolving the system by $\Delta t$ is of the order of $\Delta t^4$, even if third derivatives do not appear explicitly. This algorithm is at the same time simple to implement, accurate and stable, explaining its large popularity among molecular dynamics simulators.

A problem with this version of the Verlet algorithm is that velocities are not directly generated. While they are not needed for the time evolution, their knowledge is sometimes necessary. Moreover, they are required to compute the kinetic energy 'K', whose evaluation is necessary to test the conservation of the total energy, E = K+V. This is one of the most important tests to verify that a MD simulation is proceeding correctly. One could compute the velocities from the positions by using;

$$v(t) = \frac{r(t + \Delta t) - r(t - \Delta t)}{2\Delta t} \tag{12}$$

However, the error associated to this expression is of order $\Delta t^2$ rather than $\Delta t^4$.

To overcome this difficulty, some variants of the Verlet algorithm have been developed. They give rise to exactly the same trajectory, and differ in what variables are stored in memory and at what

times. The leap-frog algorithm is one of such variants [68] where velocities are handled somewhat better.

An even better implementation of the same basic algorithm is the so-called "velocity verlet" scheme, where positions, velocities and accelerations at time t+Δt are obtained from the same quantities at time t in the following way:

$$r(t + \Delta t) = r(t) + v(t)\Delta t + (1/2)a(t)\Delta t^2$$

$$v(t + \Delta t/2) = v(t) + (1/2)a(t)\Delta t$$

$$a(t + \Delta t) = - (1/m)\nabla V(r(t + \Delta t))$$

$$v(t + \Delta t) = v(t + \Delta t/2) + (1/2)a(t + \Delta t)\Delta t \qquad (13)$$

### 3.7.2 The Predictor-Corrector Algorithm

Predictor-corrector algorithms constitute another commonly used class of methods to integrate the equations of motion. Those more often used in molecular dynamics are due to Gear, and consists of three steps:

*1. Predictor*. From the positions and their time derivatives up to a certain order 'q', all known at time 't', one "predicts" the same quantities at time 't+Δt' by means of a Taylor expansion. Among these quantities are, of course, accelerations 'a'.

*2. Force Evaluation*. The force is computed taking the gradient of the potential at the predicted positions. The resulting acceleration will be in general different from the "predicted acceleration". The difference between the two constitutes an "error signal".

*3. Corrector*. This error signal is used to "correct" positions and their derivatives. All the corrections are proportional to the error signal, the coefficient of proportionality being a "magic number" determined to maximize the stability of the algorithm.

## 3.8 ENSEMBLES

An ensemble is a collection of all the possible states of a real system. Several methods are available for controlling temperature and pressure. Depending on which state variables (the energy E, enthalpy H (that is, U+PV), number of particles N, pressure P, stress S, temperature T, and volume V) are kept fixed, different statistical ensembles can be generated as follows:

Constant Number of particles, constant temperature and constant pressure (NPT)

Constant Number of particles, constant temperature and constant volume (NVT)

Constant Number of particles, constant volume and constant energy (NVE)

Constant Number of particles, constant pressure and constant enthalpy (NPH)

### 3.8.1 NPT ensemble

The constant number of particles, constant-temperature, constant-pressure ensemble (NPT) allows control over both the temperature and pressure. The unit cell vectors are allowed to change, and the pressure is adjusted by adjusting the volume. Pressure can be controlled by the Berendsen, Andersen, or Parrinello-Rahman method. Temperature can be controlled by any method available i.e. Nose-Hoover, Andersen, or Berendsen. NPT is the ensemble of choice when the correct pressure, volume, and densities are important in the simulation. NVT ensemble NVT ensemble is obtained by controlling the temperature through direct temperature scaling during the initialization stage and by temperature-bath coupling during the data collection phase. Temperature controlled MD simulation is important in several types of systems.

### 3.8.2 NVE ensemble

NVE the pressure and temperature is not controlled during the simulation. The main objective is to conserve the energy. However, this might cause the pressure or temperature overshoot during time integration process. Typically, a system with higher stability is suitable for NVE. Thermodynamically systems following NVE ensemble are insulated from the surrounding environment.

### 3.8.3 NPH ensemble

Enthalpy H, which is the sum of U and PV, is constant when the pressure is kept fixed without any temperature control. Although the temperature is not controlled during NPH dynamics, it is possible to use these conditions during the equilibration phase of simulation. For this purpose, it is possible to hold the temperature within specified tolerances by periodic scaling of the velocities.

## 3.9 GENERAL PROCEDURE OF MOLECULAR DYNAMICS SIMULATION

Define initial positions and velocities $\vec{r}_i(t_0)$ and $\vec{v}_i(t_0)$

Calculate forces at current time $t_n$:
$$\vec{F}_i = -\vec{\nabla}_i U(\vec{r}_1, \vec{r}_2, \vec{r}_3, ..., \vec{r}_{N_{at}})$$

Solve equations of motion for all particles in the system over a short timestep $\Delta t$.
$$\vec{r}_i(t_n) \rightarrow \vec{r}_i(t_{n+1}) \qquad \vec{v}_i(t_n) \rightarrow \vec{v}_i(t_{n+1})$$
$$t_{n+1} = t_n + \Delta t$$

Calculate desired physical quantities, write data to trajectory file $\longrightarrow$ Is $t_{n+1} > t_{max}$ ?

Write to the disc final atomic configuration & finish
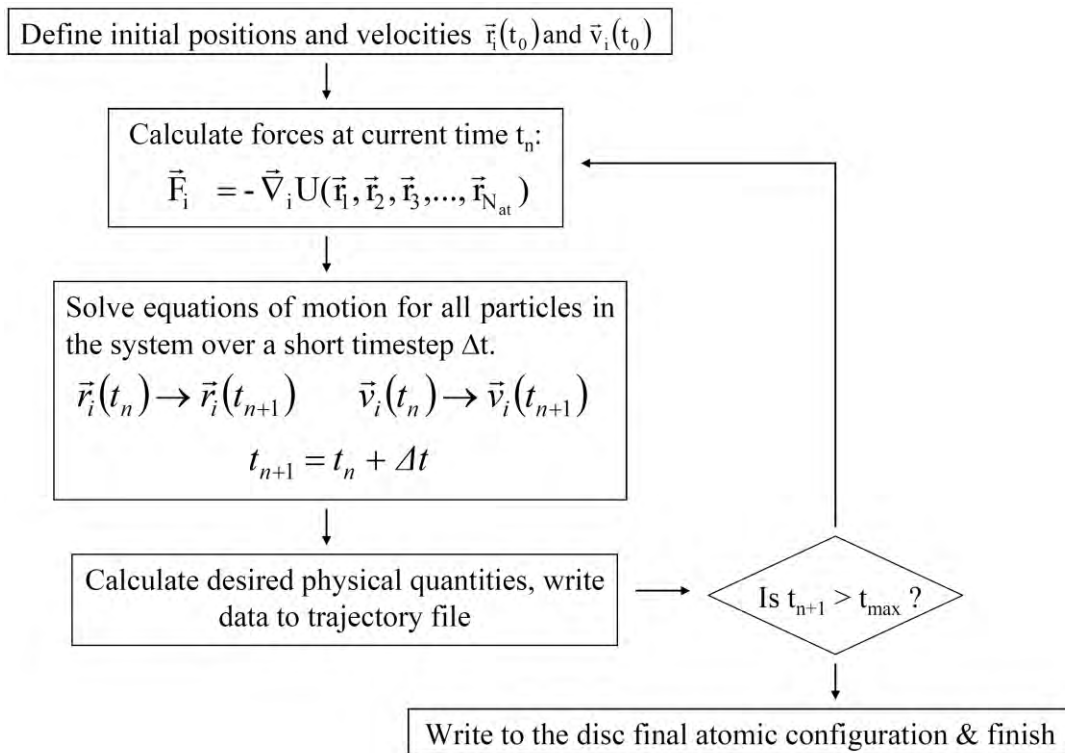
Figure 5:  Schematic diagram of a basic MD code

# CHAPTER 4

# MODELLING AND SIMULATION PROCEDURES

## 4.1 MODELLING THE SIMULATION DOMAIN

The molecular system adopted for this study consists of liquid films sandwiched between two parallel solid walls separated by few nanometer distances. The gap thickness, (h) between the solid walls was varied from 0.585 nm to 27.788 nm. Three monolayers of solid molecules, each layer having 578 molecules were placed at the bottom and at the top of the $6.14 \times 6.14 \times h$ nm$^3$ simulation box; arranged in fcc (100) lattice corresponding to a density of 8960 kg/m$^3$, which resembles Cu molecules. Liquid molecules were filled between the solid walls corresponding to a density of 1320 kg/m$^3$, which resembles liquid Ar. Temperature of the simulation domain was varied from 100 K to 150 K i.e. the fluid Ar during the simulation domain always remained in its liquid phase. Figure 6 presents the details of the simulation domain used for this study.
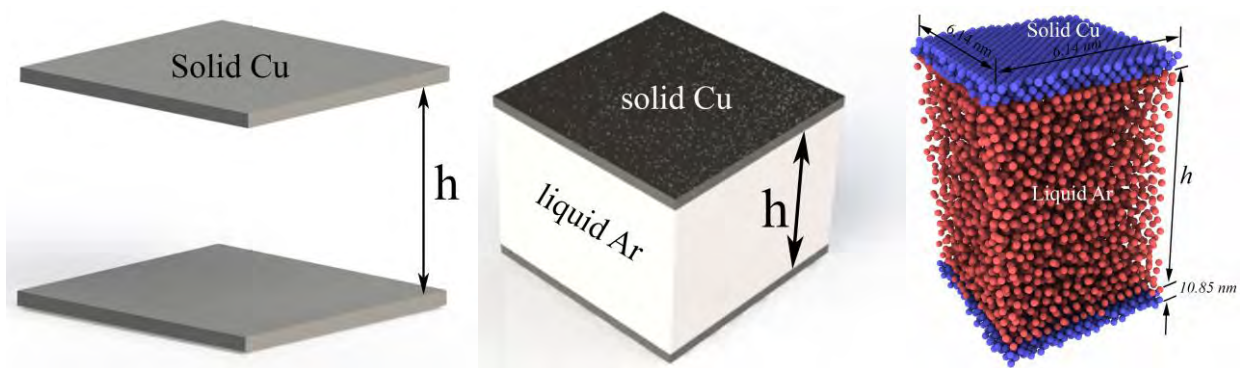


Figure 6: Initial configuration of the simulation domain (a) schematic without liquid Ar (b) schematic with liquid Ar (c) atomistic view of the model.

For atom to atom interaction, the simplified Lennard-Jones (LJ) model was employed in this simulation. Previous research reveals that results from the simplified LJ model and atomically realistic models are quantitatively equivalent [37]. Lennard-Jones (LJ) $6 - 12$ potential was used to model the van der waals interactions between solid-solid, solid-liquid and liquid-liquid interaction with a cutoff distance of $2.5\sigma$. The truncated LJ potential used for this study is:

$$\phi_{truncated}(r_{ij}) = 4\epsilon \left[ \left( \left( \frac{\sigma}{r_{ij}} \right)^{12} - \left( \frac{\sigma}{r_{ij}} \right)^6 \right) - \left( \left( \frac{\sigma}{r_c} \right)^{12} - \left( \frac{\sigma}{r_c} \right)^6 \right) \right] \qquad (14)$$

Where,

$r_{ij}$ is the intermolecular distance

ε is the depth of the potential well

σ is the molecular diameter

$r_c$ is the cutoff radius [40]

<p align="center">Table 1: Lennard-Jones interaction parameters</p>

| Pair Interaction | $\epsilon_{ij}$ (J) | $\sigma_{ij}$ (nm) |
|---|---|---|
| Liquid-Liquid | $1.67 \times 10^{-21}$ | 0.3405 |
| Solid-Solid | $6.59 \times 10^{-20}$ | 0.234 |

Interaction potential's length and energy parameters used for the simulation are presented in table 1 which was collected from [34] to resemble the liquid as Ar and Solid as Cu.

Lorentz-Berthelot mixing rule was employed to calculate the LJ parameters for solid-liquid interactions [41]:

$$\sigma_{ij} = \frac{\sigma_{ii} + \sigma_{jj}}{2} \qquad (15)$$

$$\epsilon_{ij} = \sqrt{\epsilon_{ii}\epsilon_{jj}} \qquad (16)$$

The equations of motions were integrated using velocity-verlet algorithm with 5 fs time step. Periodic boundary conditions were imposed laterally (x and z directions).

To avoid the drifting of solid molecules, only bottom layer of the bottom wall and top layer of the top wall were allowed to vibrate around their fixed lattice position by applying a spring force of $57\sigma/\epsilon^2$ to each molecule of that layer. The next layer of the solid wall was used as the thermal bath. Temperature of the solid wall was controlled by controlling velocity of this layer using the Nose-Hoover thermostat. From its initial configuration, the simulation was run for 1 ns switching on Nose-Hoover thermostat at 100 K. The simulation domain reached equilibrium within this time step. This step was followed by a relaxation period where the simulation domain was allowed to run for 1 ns switching off the entire thermostat. At the end of the relaxation period when the simulation reached its equilibrium state, the ensemble average of the total energy and the temperature of the liquid layer were evaluated for another 2 ns.

## 4.2 FORMULATION OF THERMAL TRANSPORT PROPERTIES

Heat capacity of the bulk liquid was determined by two methods: one is finite difference technique and the other is fluctuation formula - both of which are based on the classical laws of thermodynamics [40] which relates heat capacity of a substance with its heat content or energy content and temperature,

$$C_v = \left(\frac{\partial Q}{\partial T}\right)_{V,N} = \left(\frac{\partial E}{\partial T}\right)_{V,N} \tag{17}$$

Where, 'E' is the total energy and 'T' is the temperature of the system under consideration with constant volume, 'V' and number of atoms, 'N'.

The centered finite difference (cfd) technique is based on the discretization of this classical equation. In this method, one runs a simulation at the state point defined by (V, T), then two other simulations at (V, T + $\epsilon$) and (V, T − $\epsilon$). The choice of $\epsilon$ is made so that one can observe statistically valid differences in the total energy between the state points [42]. Thus, the heat capacity at constant volume, $C_v$ can be determined as:

$$C_v = \frac{E(V,T+\epsilon) - E(V,T-\epsilon)}{2\epsilon} \tag{18}$$

The other method, named fluctuation formula uses statistical thermodynamics to evaluate heat capacity of a pure substance. Thermodynamic properties that correspond to partial derivatives can be calculated from statistical thermodynamics based on fluctuations in the NVT ensemble [40]. The constant volume heat capacity is proportional to the variance of the energy:

$$C_v = \frac{var(E_T)}{K_B T^2} \tag{19}$$

Where, '$E_T$' is the Total Energy, '$K_B$' is the Boltzmann constant and 'T' is the ensemble averaged temperature of the system under consideration.

The value of $C_v$ for the bulk liquid was computed using both of these formulae and compared with the existing data available from literature [43] and NIST database [44].

Heat capacity of the nanoconfined liquid was determined using fluctuation formula. Once the simulation with initial nanoconfinement gap thickness, (h) to lattice spacing, (a) ratio, h/a = 1.0 was completed ('a' is the lattice constant of liquid Ar = 0.585 nm), the entire procedure was repeated for higher h/a ratios (1.5 to 47.5) keeping the temperature constant (100 K). Simulations were also performed for different temperatures (110 to 150 K with 10 K interval) considering the fact that critical temperature, pressure and density of Ar are 150.687 K 4.8630 MPa and 535.599 kg/m$^3$ respectively [44].

Thermal resistance of the overall system ($R_{overall}$) and the liquid region ($R_{liquid}$) was calculated using Fourier's law of heat conduction:

$$R_{overall} = \frac{1}{k_{overall}} = \frac{A\tau\delta T}{\Delta E_{avg}H} \tag{20}$$

$$R_{liquid} = \frac{1}{k_{liquid}} = \frac{A\tau(\frac{\delta T}{\delta x})}{\Delta E_{avg}} \tag{21}$$

where 'A' is the cross-sectional area, '$\tau$' is the simulation time, 'H' is the gap thickness between the two solid walls, '$(\frac{\delta T}{\delta x})$' is the linearized temperature gradient of the liquid region.

Interfacial thermal resistance (ITR) was calculated using equations (20) and (21).

The molecular diffusion was analyzed through the time evolution of the mean squared displacement (MSD) which is defined as [45];

$$MSD(\tau) = < \Delta r(\tau)^2 > = < |r_i(t + \tau) - r_i(t)|^2 > \tag{22}$$

where 'r(t)' is the position of the particle at time 't', and '$\tau$' is the lag time between the two positions taken by the particle used to calculate the displacement $\Delta r(\tau) = r_i(t + \tau) - r_i(t)$. The average <...> designates a time-average over 't' and/or an ensemble-average over several trajectories.

The self-diffusion constant, 'D' of the liquid Ar was calculated taking the limiting slope of MSD(t),

$$D_{lq} = \frac{1}{\delta} \lim_{t \to \infty} \frac{d < |r_i(t) - r_i(t_o)|^2 >}{dt} \tag{23}$$

where $\delta$ depends on the space dimensionality (6 for three dimensions).

Phonon mean free path '$l$' in liquid Ar film for the specified state of the liquid was calculated using the formula [46],

$$l = \frac{\bar{v}}{z} = \frac{k_B T}{\sqrt{2}\sigma p} = \frac{k_B T}{\sqrt{2}(\pi d^2)p} \tag{24}$$

Where '$\bar{v}$' is the average speed of phonon, 'z' is the collision frequency, 'T' is the mean temperature of the liquid film, '$\sigma$' is collision cross section, 'p' is the average pressure of the liquid film and 'd' is the collision diameter of liquid Ar molecule.

The standard values of collision diameter, 'd' for liquid Ar was taken to be 0.33 $nm$ [46] and collision cross section, $'\sigma'$ was 0.342 $nm^2$ [46]. This yielded the mean free path of liquid Ar to be around 6 nm for the 100 K case.

All the simulations presented in this study were performed using LAMMPS [47], visualization was done using OVITO [48].

# CHAPTER 5
# EFFECT OF GAP THICKNESS ON HEAT CAPACITY OF LIQUID

## 5.1 INTRODUCTION

The physical properties of liquids are known to change dramatically as the degree of confinement approaches to molecular dimensions [1]. For example, a liquid's viscosity can increase by several orders of magnitude in films with molecular or "nanoscale" dimensions. The "structure" of a liquid can also change, becoming more ordered, solid-like, or even crystalline or less ordered and more fluid-like than the bulk liquid, depending on how the microscopic shape and atomic structure of the confining walls match that of the liquid molecules [1] which in-fact depends on the film thickness of the liquid entrapped in between the solid walls. So, it is expected that variations of gap thickness will have a profound effect on heat capacity of the confined liquid.

Understanding the behavior of fluids and their manipulation within nanoscale confinement is of great interest for a vast number of applications that include the design of micro/nano electromechanical systems, microfluidic device components, and computer hard drives. Fluids inside the nanoscale channels can exhibit substantially different physics from what is observed in larger-scale systems because of the breakdown of the continuum hypothesis as well as the increased influence of the wall-force field effects [15]. To aid in the design of devices employing thin films, accurate models for the film thermal transport properties are required. Superlattices, periodic materials that contain films of alternating species e.g., Si and Ge with thicknesses as small as 1 nm, are being studied for their potential to increase the efficiency of thermoelectric energy conversion devices [12] These film thicknesses are less than the mean free paths of many of the phonons i.e., quantized lattice vibrations that dominate the thermal transport in semiconductors in the corresponding bulk material. From the perspective of convectional theory, the smaller the size of the device is, the higher the efficiency of convective heat transfer can be achieved. In other words, micro/nanoscale heat transfer brought up a promising opportunity to dramatically improve efficiency of thermal control if the scale of a device is miniaturized significantly [11].

This chapter begins with checking the simulation domain for thermodynamic equilibrium and with justifying the liquid phase of the fluid under confinement. The later part of this chapter deals with the heat capacity of the bulk liquid Ar for different film thickness of the liquid Ar at constant temperature (100 K) and compares the obtained simulated results with that available from existing literatures [43] and NIST [49] database. In next part, heat capacity of nanogap confined liquid for gap thickness ranging from 0.585 nm to 27.8 nm (h/a=1.0 to 47.5) at constant temperature (100 K) have been investigated. Lastly, the possible reasons behind this unusual behavior of thermal transport have been analyzed.

## 5.2   CHECK FOR EQUILIBRIUM AND PHASE

From its initial state, the simulation was run in microcanonical ensemble for 10 ns to equilibrate position of the atoms. Then the simulation domain was switched to canonical ensemble for another 5 ns turning on the Noose-Hoover thermostat to equilibrate temperature of the whole simulation domain. During this relaxation period, liquid region was continuously monitored which ensured that equilibrium state was reached. Figure 7 shows only two cases - one for bulk and the other for nanoconfined liquid both having same liquid film thickness (4.1 nm) and temperature (100 K). The bulk liquid indicates only the liquid Ar i.e. without any confinement or support (As LAMMPS can take care of liquids without any container or support) whereas the nanogap confined liquid refers to liquid entrapped in molecular scale confinement (As shown in Figure 6 (c)). For the rest of the cases, similar graphs have been obtained. From Figure 7 it is evident that the variation of temperature and total energy with time is considerably small indicating that the simulations are in their equilibrium state.
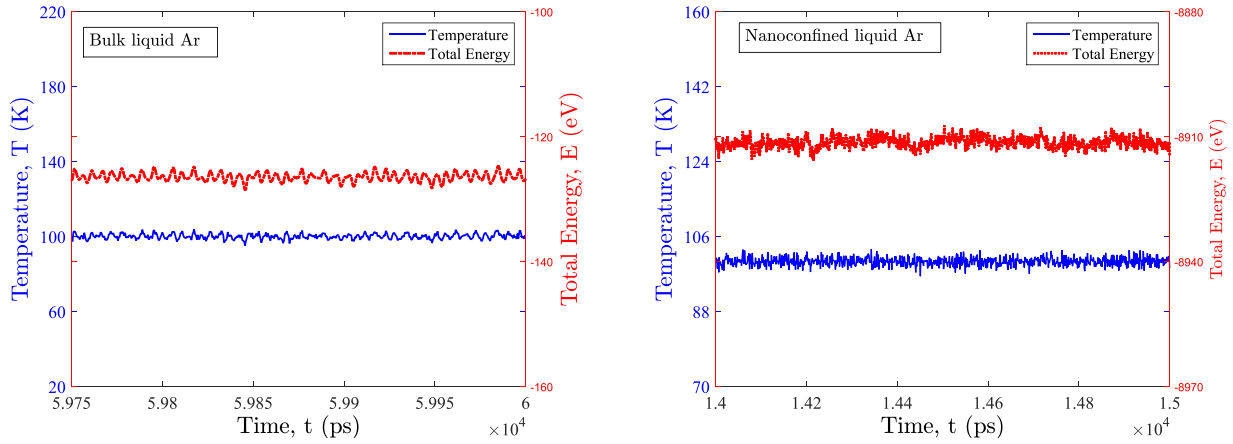
Figure 7: Fluctuation of temperature and total energy with time for a liquid film thickness of 4.1 nm

Heat capacity of liquid varies significantly from that of gaseous, critical or supercritical fluid. That is why for each case of the simulation, after equilibrium condition was reached, the temperature and pressure of the liquid domain was checked to ensure that at that specified state (density=1320 kg/m$^2$ and Temperature as specified), the fluid remained liquid all the time. From the reduced phase diagram (P/P$_c$ -T/T$_c$) of Ar [50] (Figure 8) it was seen that throughout the simulation time domain for both the bulk (P/P$_c$~5.54; T/T$_c$~0.7) and nanoconfinement conditions (P/P$_c$~ 6.71; T/T$_c$~0.7), the fluid was always in its liquid phase as expected.
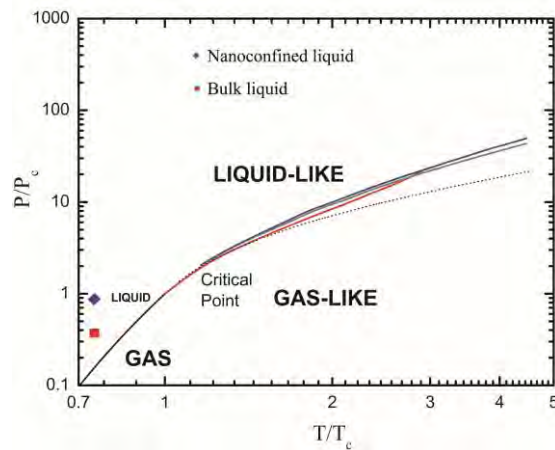


Figure 8: Reduced phase diagram (P /Pc − T /Tc) for Ar (for h/a=7.0 case). (Ref. [50])

35

## 5.3 EFFECT OF LIQUID HEIGHT ON HEAT CAPACITY-BULK LIQUID (VALIDATION OF THE METHOD USED)

The value of heat capacity for the bulk liquid Ar was determined by both fluctuation formula (equation 19) and finite difference method (equation 18) and compared with existing data from literature [43] as shown in Figure 9. All the equations for the best fit lines are within 99% confidence bounds and with reasonable RMSE values which justifies the plot. Both the methods adopted here show reasonable accuracy in determining heat capacity of the bulk liquid Ar which validate its use to determine heat capacity of the nanogap confined liquid whose data is not available in existing literature as far as the author knows. As the fluctuation formula matches closer to the NIST data, for the nanoconfinement case, it has been utilized to evaluate heat capacity at constant volume.



Figure 9: Variation of heat capacity of the bulk liquid with film thickness of the liquid.

## 5.4 EFFECT OF GAP THICKNESS ON HEAT CAPACITY-NANOCONFINED LIQUID

While heat capacity of the bulk liquid has been well understood by the researchers through experiments, the experimental work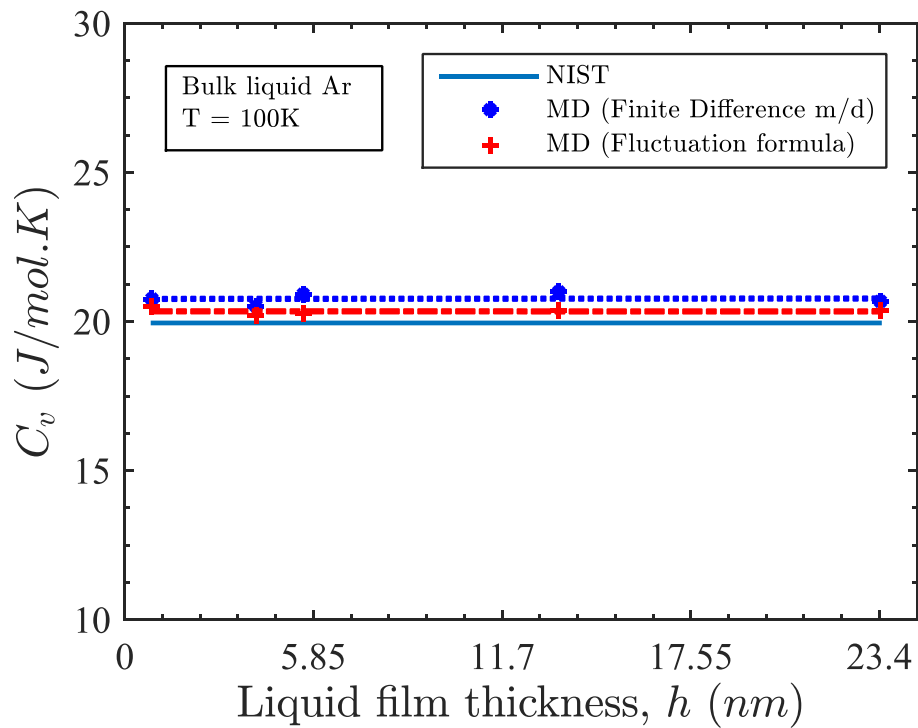 on confined liquid is rare. One reason for the scarcity of confinement liquid's data is that with our present technology it is difficult to accurately measure these properties in such small scale. An alternative way to generate these physical properties is through molecular simulation.
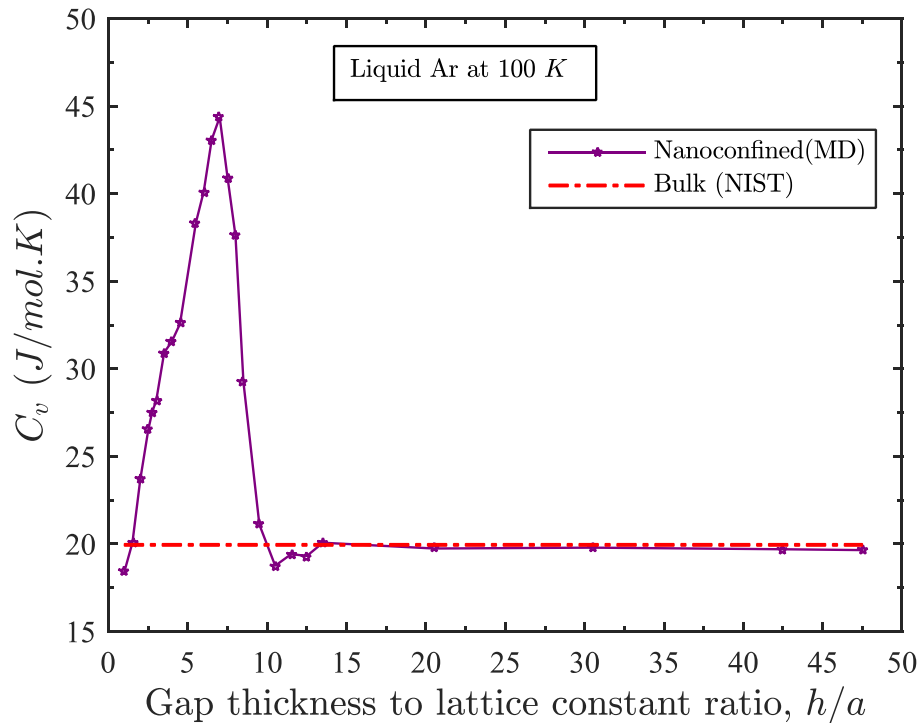


Figure 10: Variation of heat capacity with gap thickness when temperature of the nanoconfined liquid is 100 K

Heat capacity ($C_v$) of the confined liquid for varying gap thickness is presented in Figure 10. As can be observed from the figure, for a constant temperature (100 K, in this case) heat capacity of the confined liquid is different than the bulk liquid, however, as the gap thickness increases more than 10.5a (6.14 nm), heat capacity of the confined liquid approaches to that of the bulk liquid. When the gap thickness is less than 10.5a, heat capacity of the confined liquid starts to increase with the decrease of the gap thickness, reaches a peak value of about 44.8 J/mol. K at a gap thickness of 7a (4.1 nm), and eventually becomes closer to that of the bulk liquid when the gap thickness decreases to a value of 1.5a (0.8775 nm).

## 5.5 POSSIBLE REASONS BEHIND THIS ANOMALOUS BEHAVIOR

Heat capacity of a substance is a direct function of its internal energy. Internal energy i.e. heat capacity of a material can be observed to depend on three factors- (1) The average energy of each phonon (2) Average number of phonons existing at that temperature and (3) Modes of vibration at that temperature. More specifically, for liquid, heat capacity is the sum of two contributions: vibrational and configurational [51]. The vibrational contribution arises from the excitation of mechanical degrees of freedom, and the configurational contribution arises from a change in the liquid's structure. Both contributions are interdependent and vary with the volume and the structure of the liquid.

For nanoconfined liquid, along with these facts, some additional and more complex phenomenon arise resulting in anomalous behavior of its heat capacity. To figure it out, four aspects of nanoconfined liquid were focused (i) configurational change of nanoconfined liquid (ii) phonon transport mechanism (iii) mode of energy transfer (iv) interfacial thermal resistance and (v) Guided molecular motion.
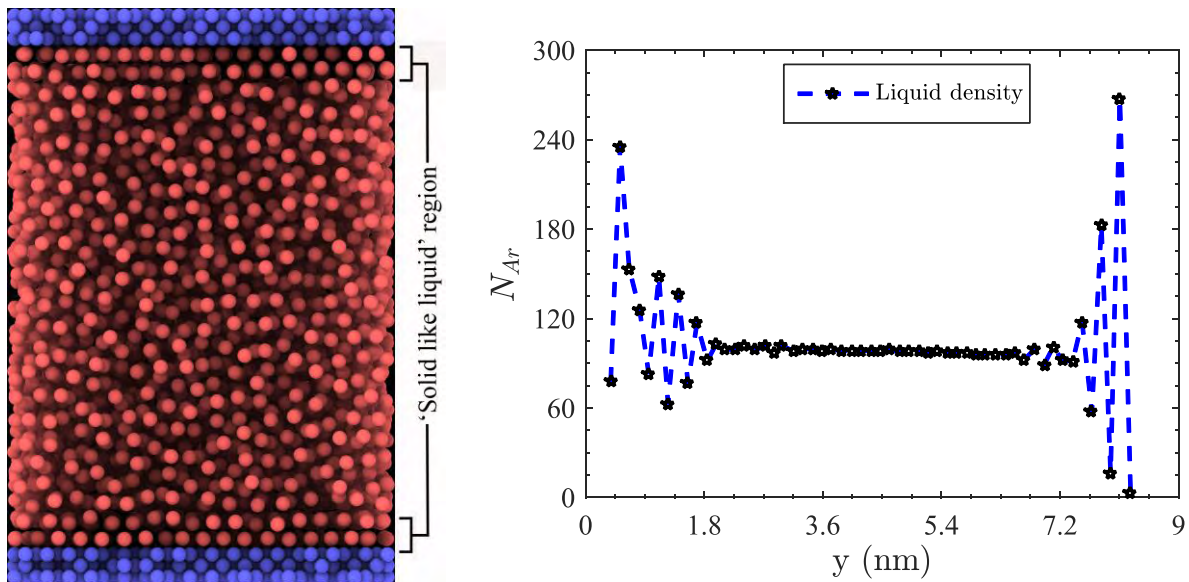


Figure 11: (a) Density profile of the nanoconfined liquid (b) Density distribution within the simulation domain (Rendered from xz plane)

The configurational change of nanoconfined liquid is due to its non-uniform density distributions. The number density profile shown in Figure 11 (a) illustrates that the liquid domain consists of

three distinct regions. Liquid density exhibits strong oscillation near the wall due to the wall force field effects and local liquid-liquid interactions [52]. The density layering extends approximately 2 nm from each surface, after which the liquid Argon's density reaches nearly a constant value. Near the confinement, there is severe fluctuations of liquid density resulting in nearly zero molecules within certain bins. Liquid atoms in this region are packed like a solid structure with mobility much lower than the rest of the liquid region (Figure 11 (b)) and hence termed as 'Solid like liquid' region. The effect of the wall interaction exerted on confined liquid molecules produces a strong effect on its dynamics, which is disrupted only at very high temperatures [25]. For nanogap confinement similar phenomenon has been reported earlier [35].

The average density of the liquid molecules in the wall affected zone is high compared to that of the region far from the wall. Due to the density peak in the solid like liquid region, number of heat carrying molecules reduces in the liquid region. Moreover due to wider translational degrees of freedom, heat capacity of the liquid is larger than that of solid [8]. So, the formation of solid like liquid layer near the wall causes an overall decrease of heat capacity.

When liquid film thickness is large enough than phonon wavelength and mean free paths, phonons travel diffusively due to the resistivity of the medium through which it is being transported [25]. The resistivity exists because a phonon, while moving inside a medium, is scattered by impurities, defects, the atoms/molecules composing the medium that simply oscillate around their equilibrium position (in a solid), or, generally, by any freely-moving atom/molecule composing the medium, in a gas or liquid [25]. For a given medium a moving phonon can be ascribed a mean free path as being the average length that the electron can travel freely, i.e., before a collision, which could change its momentum. The mean free path can be increased by reducing the number of impurities in a crystal or by lowering its temperature [25]. For diffusive phonon transport, simple TCM (Thermal circuit model) works well i.e. the net thermal resistance is equal to the sum of interface thermal resistances and the film resistances [53]. Heat capacity of the confined liquid in such case is very close to that of the bulk as shown in Figure 10 for higher gap thickness.

But when gap thickness is on the order of a few nanometers that is comparable to phonon mean free path or even phonon wavelength, new phenomena such as ballistic transport [26], [54] and coherent transport [27], [28] are observed. Phonons in such cases, can travel ballistically across

material without any impedance and encounter significant scattering at the boundaries of the material which greatly reduces phonon MFPs (Mean free paths). Ballistic conduction is the unimpeded flow of charge, or energy-carrying particles, over relatively long distances in a material [26]. Ballistic transport is observed when the mean free path of phonon is (much) longer than the dimension of the medium through which the phonon travels [26]. The phonon alters its motion only upon collision with the walls. Consequently, simple TCM does not work well for this region. In such cases, thickness significantly affects the vibrational density of states (VDOS) [34]. The modification of VDOS in turn affects the net phonon transportation resulting in an increase or decrease of heat capacity of the confined liquid. Similar phenomena have been observed recently for both crystalline thin film and liquid layer [55] confined between two identical leads.

When h/a approaches to its critical value (at which $C_{v, max}$ occurs, denoted by (h/a)$^*$) phonon can preserve their coherence nature after transmitting through the interface. Across the thin film, ballistic transport occurs and in this region phonons usually have shorter mean free paths caused by diffuse boundary scattering [4], [56]. When film thickness approaches to phonon mean free paths, phonon-phonon umklapp scattering starts to dominate phonon scattering [33] which allows low transmission of phonons. All these facts suddenly contribute to an increase in heat capacity of the confined liquid.

As soon as h/a crosses its critical value, (h/a)$^*$, a further decrease in thickness suppresses some long wavelength propagation modes [25]. For such thin film, transient ballistic and diffusive phonon heat transport was previously introduced by Joshi and Majumdar [57]. The increase in phonon mean free path due to a reduction of phonon frequency causes a higher phonon transmission rate [25]. Eventually heat capacity drops as the film thickness goes beyond its critical value, (h/a)$^*$.

Mode of energy transfer in a fluid dictates molecular mobility to a great extent which is governed by the following equation [58],

$$J_y = \frac{1}{V}\left[\sum_i \left(\frac{1}{2}mv_i^2 + \phi_i\right)v_{i,y} + \frac{1}{2}\sum_i\sum_{j>i}\left[F_{ij}\left(v_i + v_j\right)\right]y_{ij}\right]$$
(24)

First part of this equation indicates energy transfer due to molecular motion and the second part due to molecular interaction.
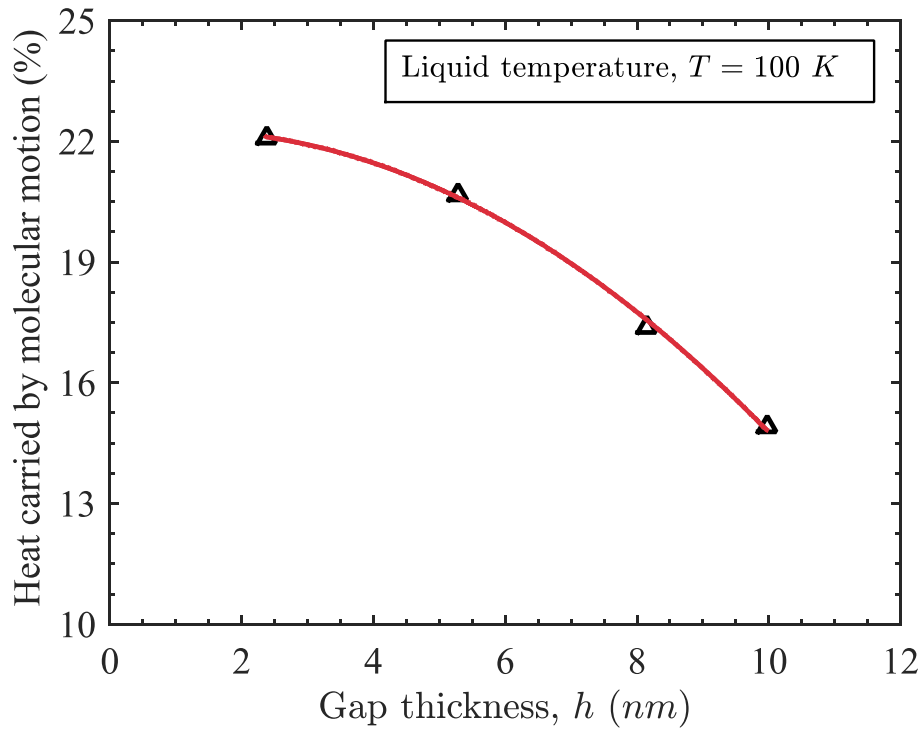
Figure 12: Mode of energy transfer of the nanoconfined liquid for different gap thickness.

Although for liquid energy transfer is due to molecular interaction, when the gap thickness decreases, the contribution of molecular motion becomes prominent as presented in Figure 12. But with the decrease of gap thickness, molecular motion starts to degrade as confined molecules have lesser degrees of freedom than the bulk and the to and fro motion of the molecules become restricted. The molecular motion is characterized with self-diffusion coefficient. Its value is less for the confined liquid compared to that of the bulk and decreases with the decrease of gap thickness as shown in Figure 13. Presence of wall affected zone and strong solid-liquid interaction force contributes to this behavioral difference of the nanoconfined liquid. Reduction in heat diffusion capability and number of heat carrying molecules results in an increase in heat capacity as h/a approaches to (h/a) *.
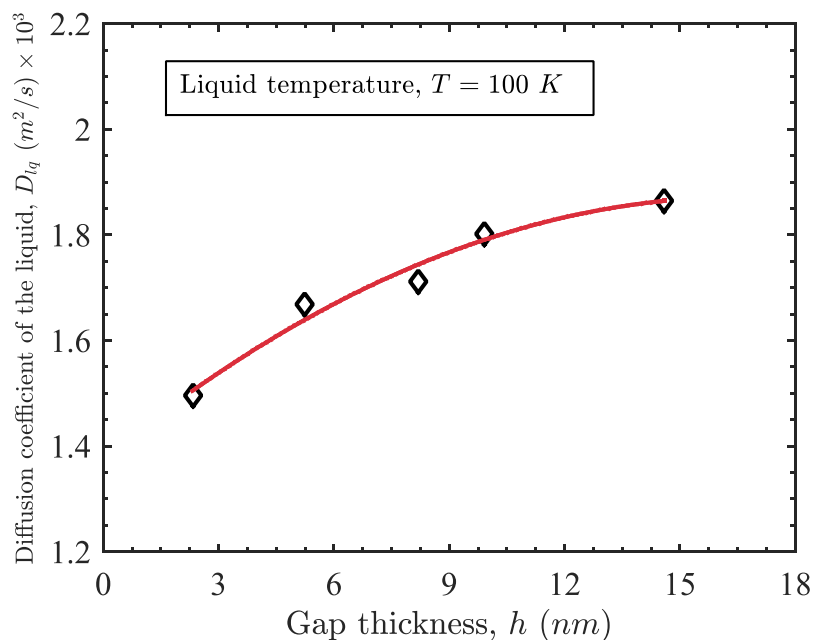
Figure 13: Diffusion coefficient of the nanoconfined liquid for different gap thickness.

Interface thermal resistance (ITR), for confined liquid, plays an important role for the anomalous behavior of heat capacity. ITR is a function of solid-liquid interaction strength, interfacial temperature but not of the gap thickness [35]. Consequently, as h/a approaches to its critical value, ITR contributes more to the overall system resistance.



Figure 14: Trajectory of a molecule's displacement at 100 K for a time period of 0.9 ns (1000 frames): (a) bulk liquid and (b) confined liquid.

Depending on confinement height, direction of molecules' motion varies. Confinement reduces chaotic to and fro motion of the liquid molecule to a guided well-defined path (Figure 14).

42

In laminar flow, fluid particles flow in an orderly manner along certain path-lines. So, the only means by which heat is transferred between different streams is through molecular diffusion i.e. movement of molecules from region of higher concentration to lower concentrat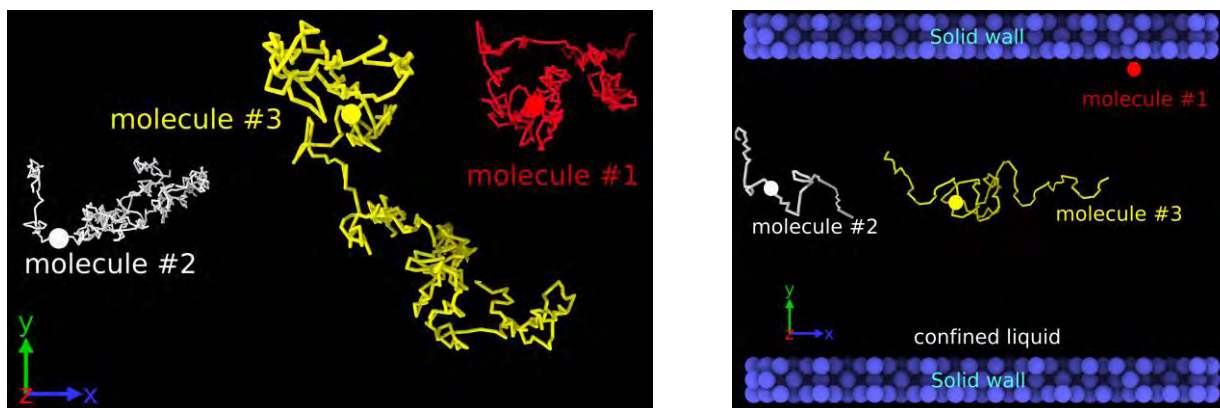ion. But in turbulent flow, the fluctuations provide an additional mechanism for heat transfer in addition to the molecular diffusion. Eddies are formed due to these fluctuations. These eddies rapidly transport mass, momentum and energy across different regions of the flow. Compared to the eddies, molecular diffusion is a very slow process and is often neglected in calculating the heat transfer rate in turbulent flows. Hence, the turbulent flows always have a higher heat transfer coefficient compared to the laminar flows. As nanogap confined liquid molecules exhibit more ordered and structured movement, transportation of heat in confined liquid is lesser than the bulk resulting in an increase in heat capacity of the confined liquid.

## 5.6 CONCLUSION

Non-equilibrium molecular dynamics simulations have been carried out to study the effect of gap thickness on heat capacity of the confined liquid. The simulation was carried out with the simplified LJ type solid-liquid molecular model; liquid molecules were confined within the solid surfaces separated by a distance varying from 0.585 nm to 27.8 nm. Heat capacity of the liquid molecules was evaluated from NEMD simulation following fluctuation formula. The result obtained from the bulk liquid is in excellent agreement with published literatures, however, a significant shift has been observed for the confined liquid. Heat capacity of the confined liquid was observed to vary significantly with nanoconfinement gap thickness, however, it follows a very complex relation to nanoconfinement gap thickness and temperature. For a limited gap thickness band heat capacity of the confined liquid is higher than the bulk liquid, beyond which, heat capacity is observed to be closely matched with the bulk liquid.

Some possible causes have been analyzed for this anomalous behavior. The nanogap confined liquid molecules are simultaneously affected by these effects. Depending on the gap thickness, one dominates others – weakening or strengthening their individual effects resulting in an increase in heat capacity when gap thickness approaches to its critical value and a decrease in heat capacity when gap thickness becomes lower than the critical value as shown in Figure 10. But qualitatively the heat capacity of nanogap confined liquid is always higher than that of its bulk counterpart although its magnitude strongly depends on the confinement gap thickness among many other factors.

# CHAPTER 6

# EFFECT OF TEMPERATURE ON HEAT CAPACITY OF LIQUID

## 6.1 INTRODUCTION

In general, transport properties of fluid significantly depends on its temperature [53], [59]. The thermal transport properties of thin liquid films are different than their corresponding bulk values as investigated by many researchers previously [12], [60], [61]. Experimental evidence of temperature-dependent heat capacity has been recently reported for metallic nanoclusters and nanodielectrics [36]. Hence it is expected that heat capacity of nanogap confined liquid will also show different behaviors with the change of liquid temperature. Interfacial interactions, symmetry breaking, structural frustration and confinement-induced entropy loss – all these factors can play dominant roles in determining transport properties like heat capacity of a physically confined liquid medium.

Temperature dependence of heat capacity of the confined liquid was studied following the procedure same as discussed in the previous section. Once heat capacity was calculated for the initial confinement temperature (100K), both the lower and the upper wall temperatures were increased by 10 K to increase the average system temperature by 10 K, keeping the liquid density constant. This represents the practical scenario where, liquid entrapped in a nanogap is subjected to different temperature environment, without allowing escape of the liquid molecules. The simulation was carried out for a temperature range 100 K to 150 K.

## 6.2  EFFECT OF TEMPERATURE ON HEAT CAPACITY-BULK LIQUID (VALIDATION OF THE METHOD USED)

With the increase of temperature molecular excitation increases resulting in greater energy transport behaviors i.e. heat capacity of the bulk liquid decreases. Existing literatures [43], [49] show a uniform decrease of heat capacity with the increase of liquid temperature. Heat capacity of the bulk liquid Ar have been determined using Finite Difference Technique and Fluctuation formula as shown in Figure 15. Both methods show good agreement with existing data [49]. As Fluctuation formula greatly matches with existing data, this method has been adopted to evaluate the heat capacity of nanogap confined liquid.
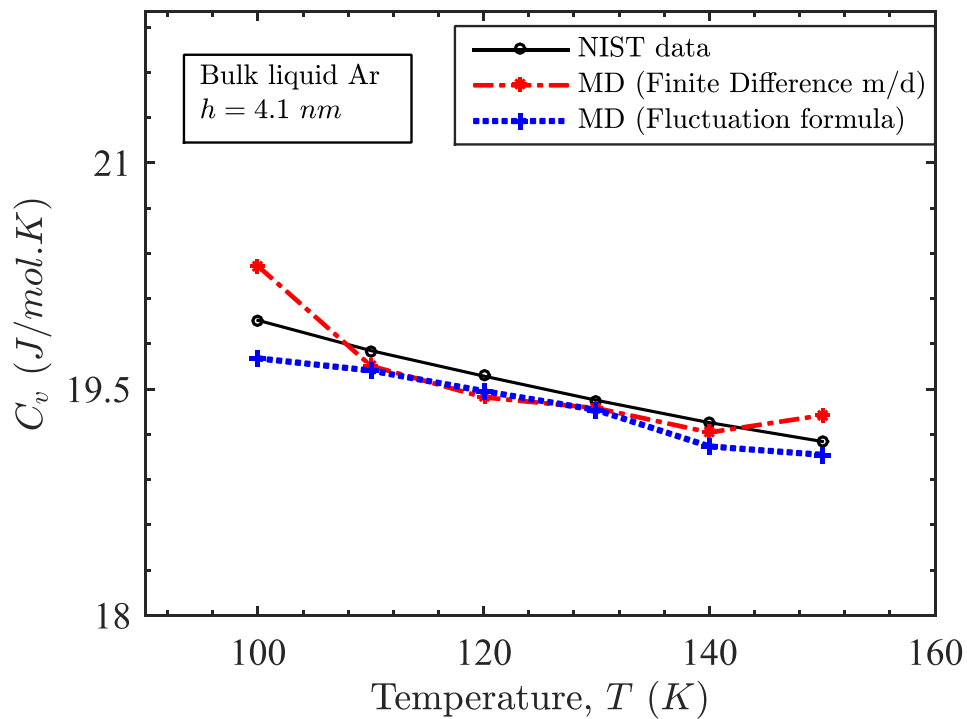


Figure 15: Variation of heat capacity of the bulk liquid with temperature

## 6.3 EFFECT OF TEMPERATURE ON HEAT CAPACITY-NANOCONFINED LIQUID

Increase in temperature decreases the heat capacity of the nanoconfined liquid too. But the rate of decrement is not as uniform as the bulk ones. Based on nanogap confined liquid height, three distinct regions have been identified for analyzing the dependence of heat capacity on temperature for confined liquid. In the first region, heat capacity of the bulk resembles to that of the nanoconfined liquid. Heat capacity of the confined liquid is always higher than the bulk in second region. In third region heat capacity of the confined liquid is higher than the bulk up-to a certain temperature after which it resembles to that of the bulk liquid.

### 6.3.1 Region-1

For gap thickness below 0.88 nm (h/a=1.5) or above 5.56 nm (h/a=9.5), confinement affects less in heat capacity of the confined liquid i.e. increasing temperature has almost same effects on nanoconfined liquid as that of the bulk. Figure 16 shows variation of heat capacity with temperature up-to a liquid height of 6.14 nm (h/a=9.5). For greater heights, similar phenomena have been observed.
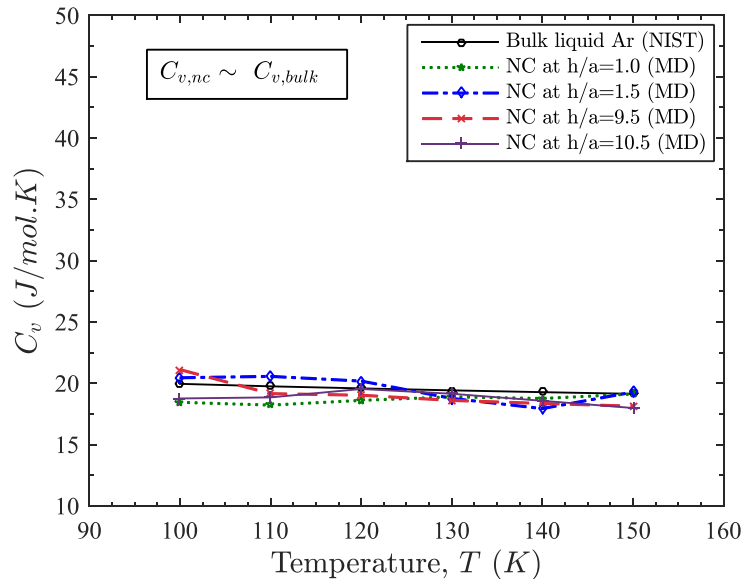


Figure 16: Variation of heat capacity of the nanogap confined liquid with temperature (Region 1: Heat capacity of the confined liquid resembles to the bulk one)

### 6.3.2 Region-2

As soon as the gap thickness increases beyond 1.2 nm (h/a=2.0), the effect of confinement starts to dominate along with the temperature of the confined liquid. Upto a confinement height of 2.63 nm (h/a=4.5), this dominance is significant. In this region, heat capacity of the confined liquid is higher than that of the bulk irrespective of the temperatures. But with the increase of temperature, heat capacity of the confined liquid in this region also shows a decreasing trend indicating the increase in transport behavior due to higher energy content at higher temperatures. Maximum heat capacity in this region can be as large as around 1.7 times than that of the bulk liquid at the same temperature. Maximum value of the heat capacity increases with that of the liquid height as seen from Figure 17.



Figure 17: Variation of heat capacity of the nanogap confined liquid with temperature (Region 2: Heat capacity of the confined liquid is higher than the bulk one)

### 6.3.3 Region-3

As the gap thickness is larger than 2.6 nm (h/a=4.5) but smaller than 5.56 nm (h/a=9.5), heat capacity of the confined liquid shows a mixed trend analogous to both region 1 and 2 i.e. upto a certain temperature it shows a higher value but beyond this temperature, its value resembles to that of the bulk liquid as shown in Figure 18. Liquid film piling up one another is thought to be responsible for this regional transport behavior of the nanoconfined liquid.
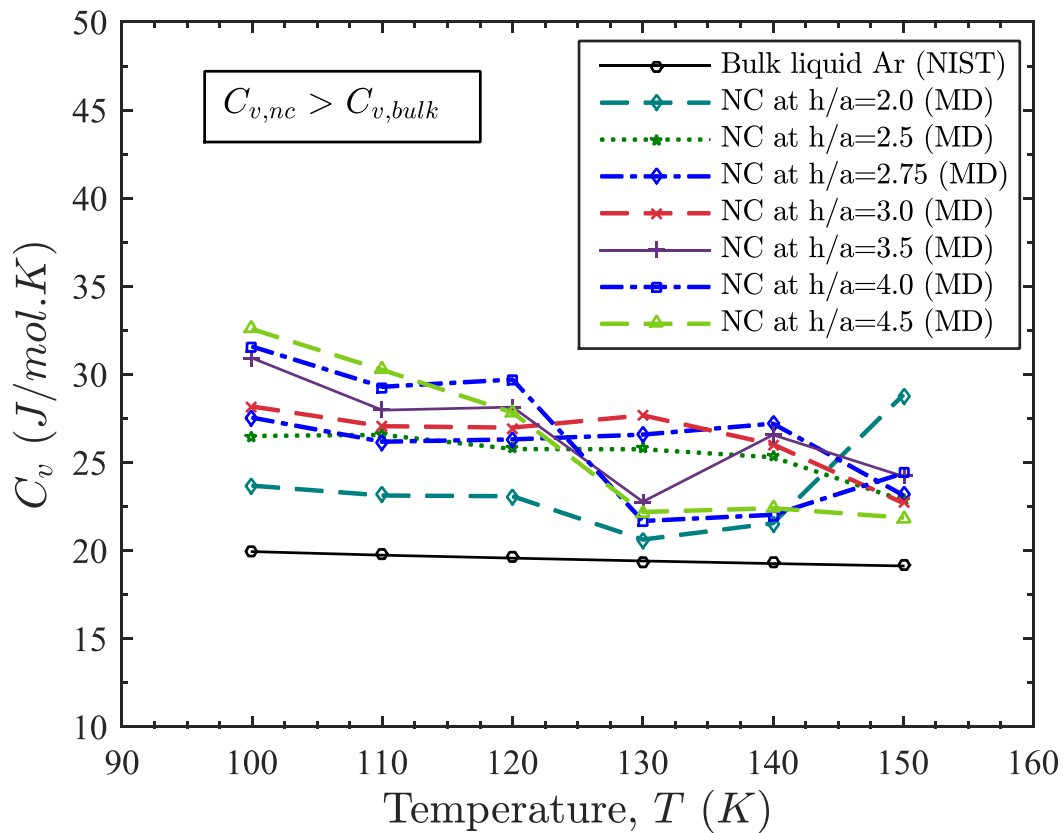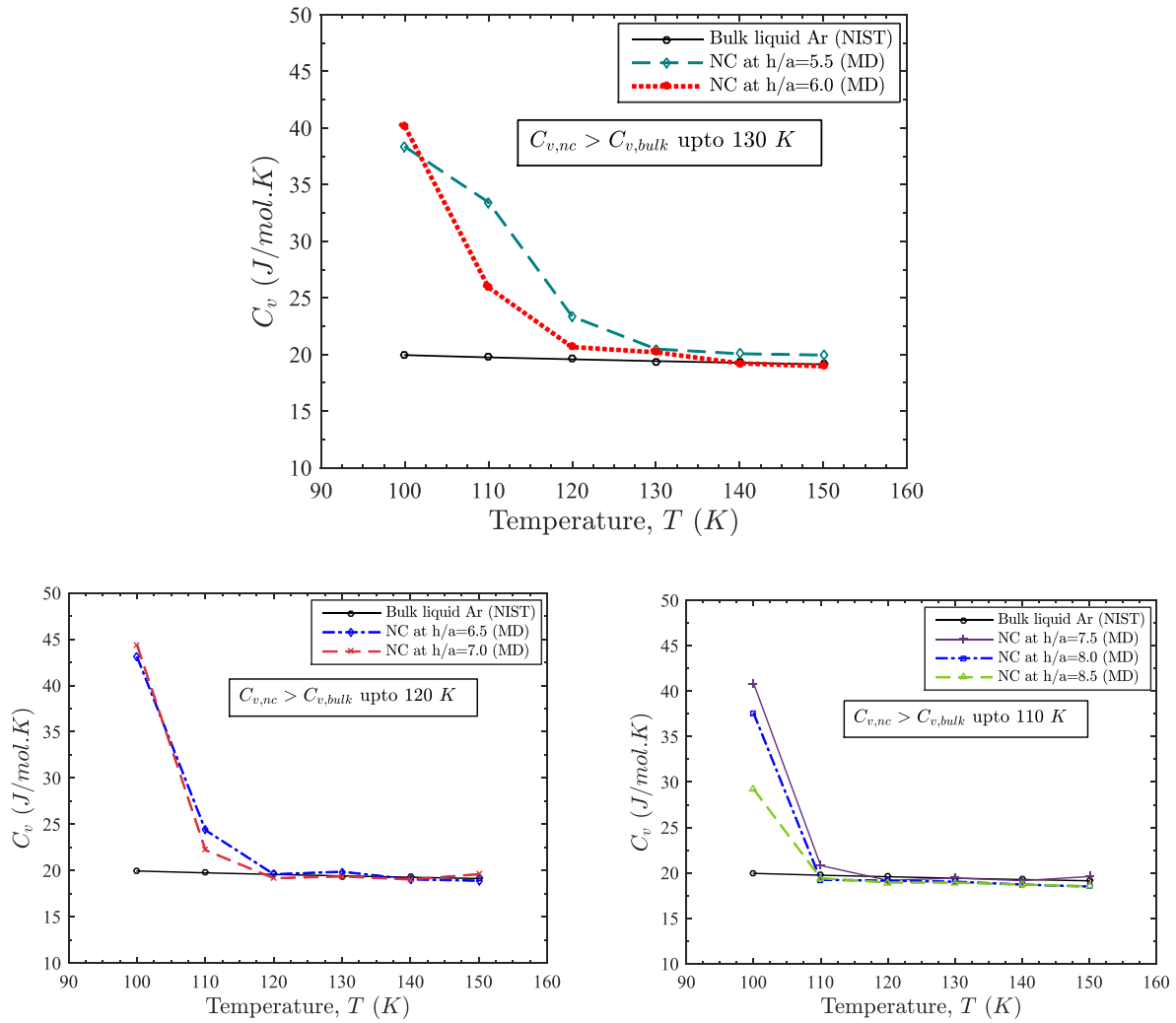


Figure 18: Variation of heat capacity of the nanogap confined liquid with temperature (Region 3: Heat capacity of the confined liquid is higher than the bulk one up-to certain temperature)

## 6.4 POSSIBLE REASONS BEHIND THIS ANOMALOUS BEHAVIOR

In general, heat capacity depends on the number of degrees of freedom that are available to the particles in a substance [62]. A degree of freedom is any form of energy in which heat transferred into an object can be stored. This can be in translational kinetic energy, rotational kinetic energy, or other forms such as potential energy in vibrational modes. The larger, the number of degrees of freedom available to the particles of a substance, the greater will be its heat capacity [62].

In contrast, quantum effects require that whenever energy be stored in any mechanism associated with a bound system which confers a degree of freedom, it must be stored in certain minimal-sized deposits (quanta) of energy, or else not stored at all [62]. If the temperature of the substance is so low that the equipartition energy (1/2 $k_B$T) is much smaller than excitation energy, there will be little or no energy in that degree of freedom and it is said to be "frozen out" [63]. Such effects limit the full ability of some degrees of freedom to store energy when their lowest energy storage quantum amount is not easily supplied at the average energy of particles at a given temperature. This is why heat capacities tend to fall at lower temperatures where the average thermal energy available to each particle's degree of freedom is smaller, and thermal energy storage begins to be limited by these quantum effects [18].
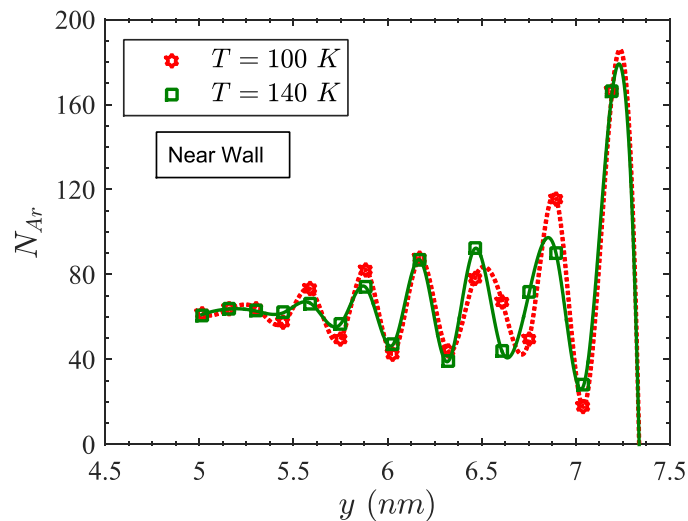


Figure 19: Density oscillation near the wall at different temperatures

For monatomic gases like Helium, Neon, Argon thermal energy comprises only translational motions. Three translational degrees of freedom (corresponding to the three independent directions in space) are available for any individual atom [18]. Accordingly, the specific heat of monatomic gas is $1/2 R \times 3 = 3/2 R = 12.4717$ J/mol.K. Surprisingly, for monatomic liquid, this value becomes $5/2 \times R = 20.79$ J/mol. K indicating the contribution of five active DOFs which is thought due to the effect of phase change.

At higher temperatures, thermal transport is predominantly provided by phonons having much lesser frequencies [36] which leads to a higher phonon transport [25]. Eventually thermal transport becomes smoother resulting in a low heat capacity as the temperature increases.

The variation of wall surface temperature, i.e. liquid temperature affects the density variation. Although, liquid layers next to the solid surface do not show any tendency for translational motion i.e. they seem like to be stuck to the solid confinement walls. Molecules in this 'solid like liquid' layer vibrate around their fixed lattice position. Number of liquid molecules remain almost unchanged in the first few layers of the solid like liquid region as is presented in Figure 19. At higher temperature, density oscillation relaxed earlier (Figure 19) and number of liquid molecules in the low-density region i.e. in the liquid region increases as shown in Figure 20. Increase in the number of heat carrying molecules in the liquid region increases heat carrying capability of the confined liquid i.e. heat capacity decreases with the increase in temperature.
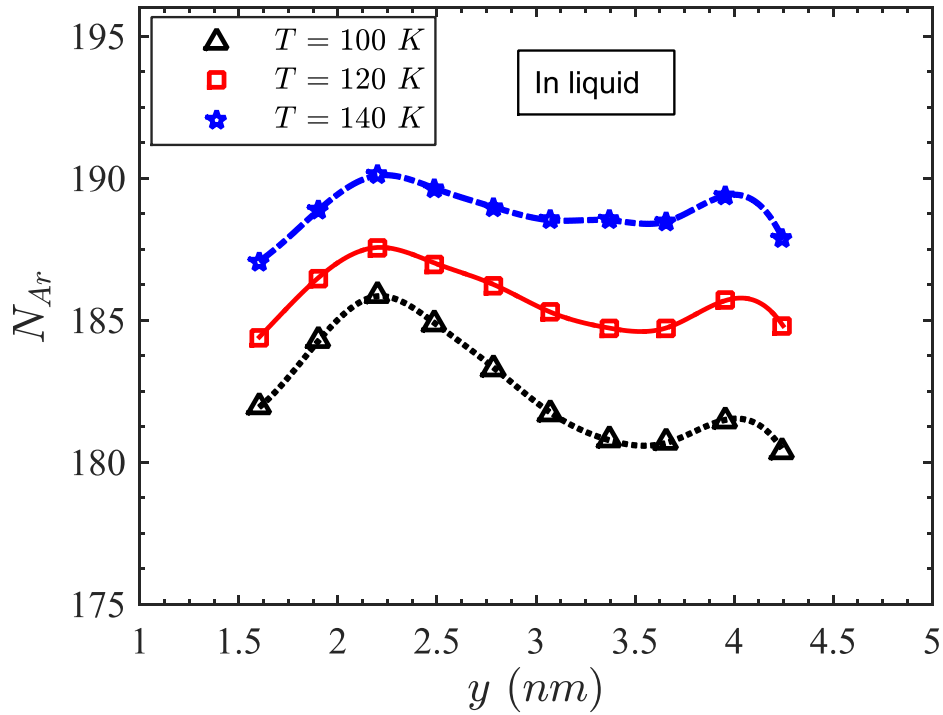
Figure 20: Number density profile at the liquid region for different system temperatures.

Heat, temperature and the motion of molecules are all inter-related. Temperature is a measure of the average kinetic energy of the molecules in a material. Heat is the energy transferred between materials that have different temperatures. Increasing the temperature increases the translational motion of molecules. Energy is related to temperature by the relationship: $E \propto T$. When heat is added to a substance, the molecules and atoms vibrate faster. As atoms vibrate faster, the space between atoms increases. The motion and spacing of the particles are determined by mean squared displacement (MSD) which is a measure of molecules' average motion over a certain period of time. Figure 21 shows that MSD increases with temperature indicating more heat is transported at higher temperatures decreasing the heat capacity of the liquid.

Figure 21: Mean squared displacement of the liquid molecules at different temperatures.
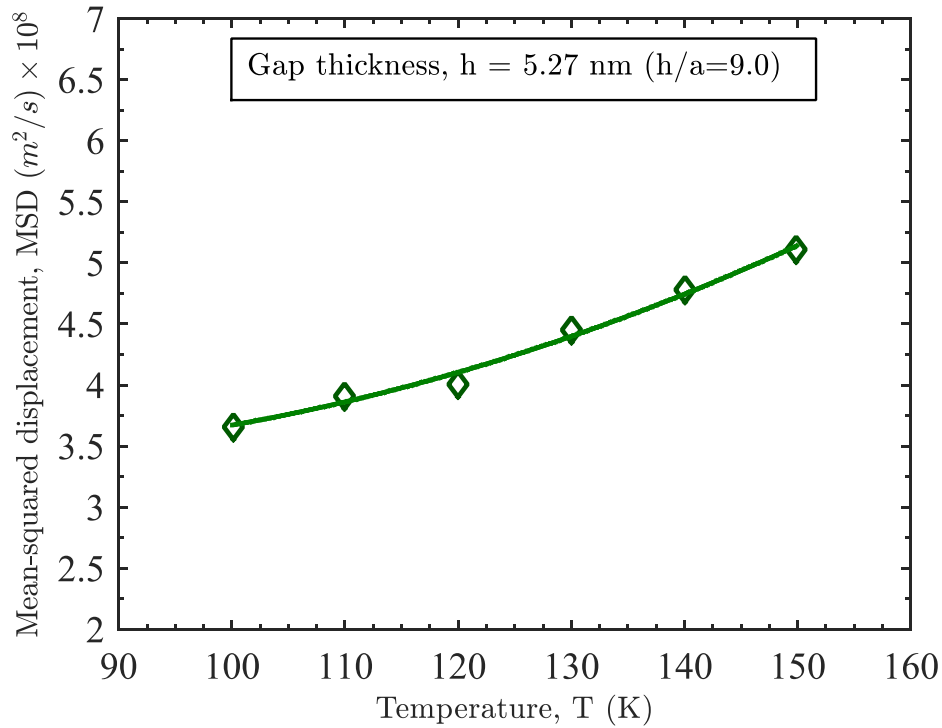
When heat flows from a solid to the in-contact liquid, a thermal resistance is experienced due to phonon scattering at the interface which is called kapitza resistance [64] or interfacial thermal resistance (ITR). For macro-scale heat transfer ITR is negligible, but when the system size shrinks to nanoscale or heat flux reaches too high, its influence is no longer negligible. Previously molecular dynamics simulation techniques were applied by a number of researchers to investigate the thermal transportation characteristics across the solid liquid interface [59], [65]. It reveals that interfacial thermal resistance (ITR) is strongly dependent on solid-liquid interaction strength, vibrational mismatch of two sides, surface wettability and interface temperature [34], [35].

Interface thermal resistance as a function of the temperature of the simulation domain is plotted in Figure 22. Interfacial thermal resistance was calculated using dT/q relation, where q was taken same to $\Delta E_{avg}/\tau$. A (equation 20 and 21) and dT was calculated by extending the solid and liquid temperatures to the interface linearly. From Figure 22, it is evident that ITR decreases with the
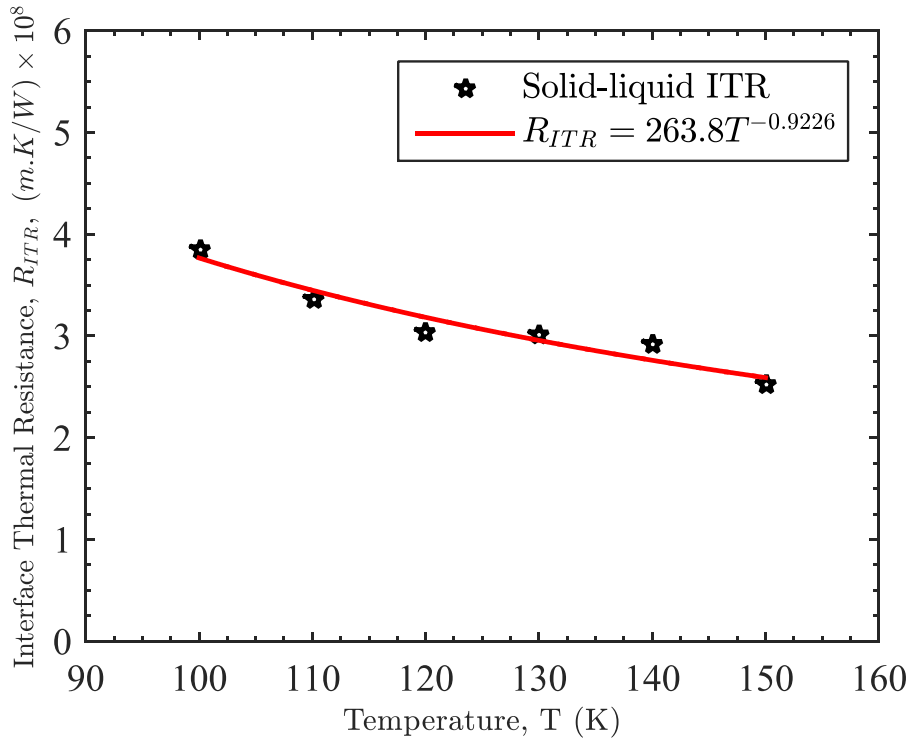
Figure 22: Variation of Interface Thermal Resistance with system temperature.

increase of temperature following a power law relation, $R_{ITR} = 263.8 \, T^{-0.9226}$. This indicates that with the increase in temperature, ITR decreases allowing more thermal energy to be transported easily decreasing the heat content of the liquid medium. ITR is also reported in previous literatures to decrease with the increase of the solid wall temperature [35], [59].

To relate ITR with overall system resistance, ITR was converted into equivalent argon's conduction layer thickness using the relation, $l_k = R_{ITR} \times k$ (Ref. [9]) for the 100 K liquid temperature with gap thickness 6.14 nm (h/a=10.5). It was found that ITR of the system to be ~3.4 nm of the confined liquid's conduction layer thickness. This value is about ~55.5% of the confined liquid's conduction layer thickness.

As mentioned previously, ITR is a function of the solid-liquid interaction potential, interfacial temperature but not of the gap thickness. As a result, with the decrease of the gap thickness ITR contributes more to the overall system resistance which results in sharper responses of overall thermal resistance with the change in temperature. Figure 23 shows that overall thermal resistance decreases with temperature differently depending on gap thickness. For a gap thickness 2.34 nm

(h/a = 4.0), it decreases with temperature following a power factor -0.8595 whereas for a gap thickness 14.63 nm (h/a = 25.0), it falls with temperature following a power factor of -0.4746. Lower value of overall thermal resistance indicates more flexibility of transportation of heat. This is why the increase in heat capacity is more prominent at low gap thickness with the decrease in liquid's temperature.
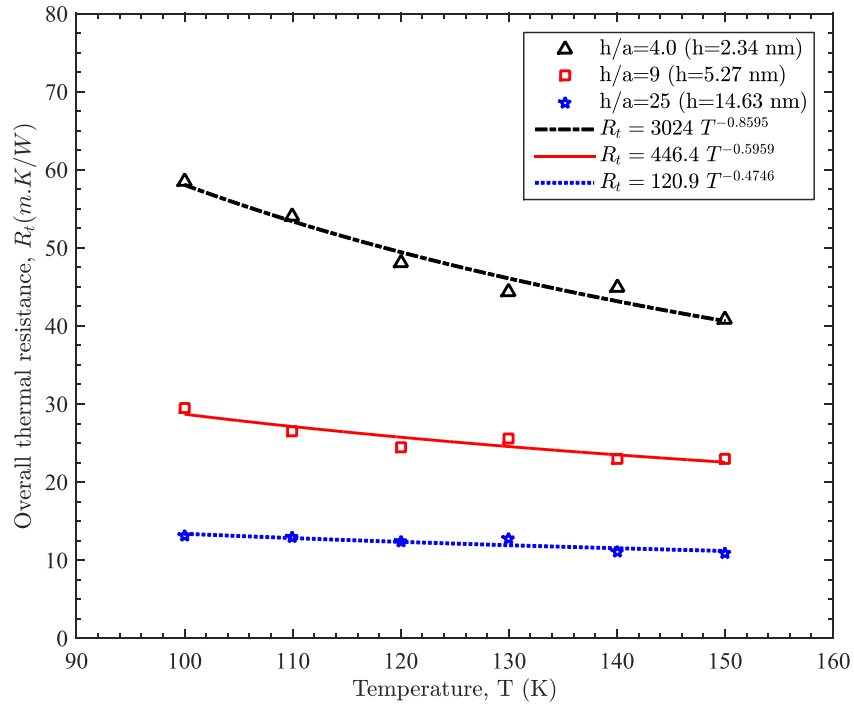


Figure 23: Temperature dependent overall thermal resistance of the nanogap confined liquid for different system temperatures.

## 6.5  CONCLUSION

Heat capacity decreases with the increase in temperature- both for bulk liquid Ar and nanogap confined liquid Ar. The variation of heat capacity with temperature is uniform for bulk liquid but in case of nanogap confined liquid, it depends on gap thickness. For a certain band of gap thickness (0.88 nm < h < 5.5 nm), heat capacity of confined liquid behaves differently than the bulk. Beyond this region, it exhibits same variation with temperature as that of the bulk liquid. This behavior is analogous to that studied earlier for solid nanoclusters by some earlier researchers. [14], [16]

# CHAPTER 7

# COMBINED EFFECT OF GAP THICKNESS AND TEMPERATURE

## 7.1 INTRODUCTION

Confined fluids are involved in several natural processes and industrial applications ranging from cellular behavior to microelectronic devices and consequently investigations of their structural and dynamic properties have received much interest in the recent literatures. In comparison to the bulk case, the characterization of the intrinsic structure of confined fluids is not straightforward. Because the interpretation of the experimental data is complicated by topological and chemical effects induced by the presence of the confining substrate. Moreover, both the temperature and the gap thickness simultaneously influence the thermodynamic behavior of such nanogap confined liquid.

In the present chapter, non-equilibrium Molecular Dynamics (NEMD) simulations has been carried out with a simplified molecular model to investigate the combined effect of gap thickness and temperature on heat capacity of nanogap confined liquid. The effect of gap thickness for a constant liquid temperature as studied in section 5.4 has been extended here for a temperature ranging from 110 K to 150 K. As the value of maximum heat capacity is of great importance for many instances, it is investigated separately. It has been found that the maximum value of heat capacity follows a complex relation with temperature and gap thickness. The temperature at which maximum heat capacity is achieved, is observed to vary with gap thickness following a power law. With a specific gap thickness and temperature, heat capacity as high as around 2.3 times than that of the bulk can be achieved in nanogap confined liquid.

## 7.2 EFFECT OF VARYING GAP THICKNESS ON HEAT CAPACITY OF CONFINED LIQUID AT DIFFERENT CONSTANT TEMPERATURES
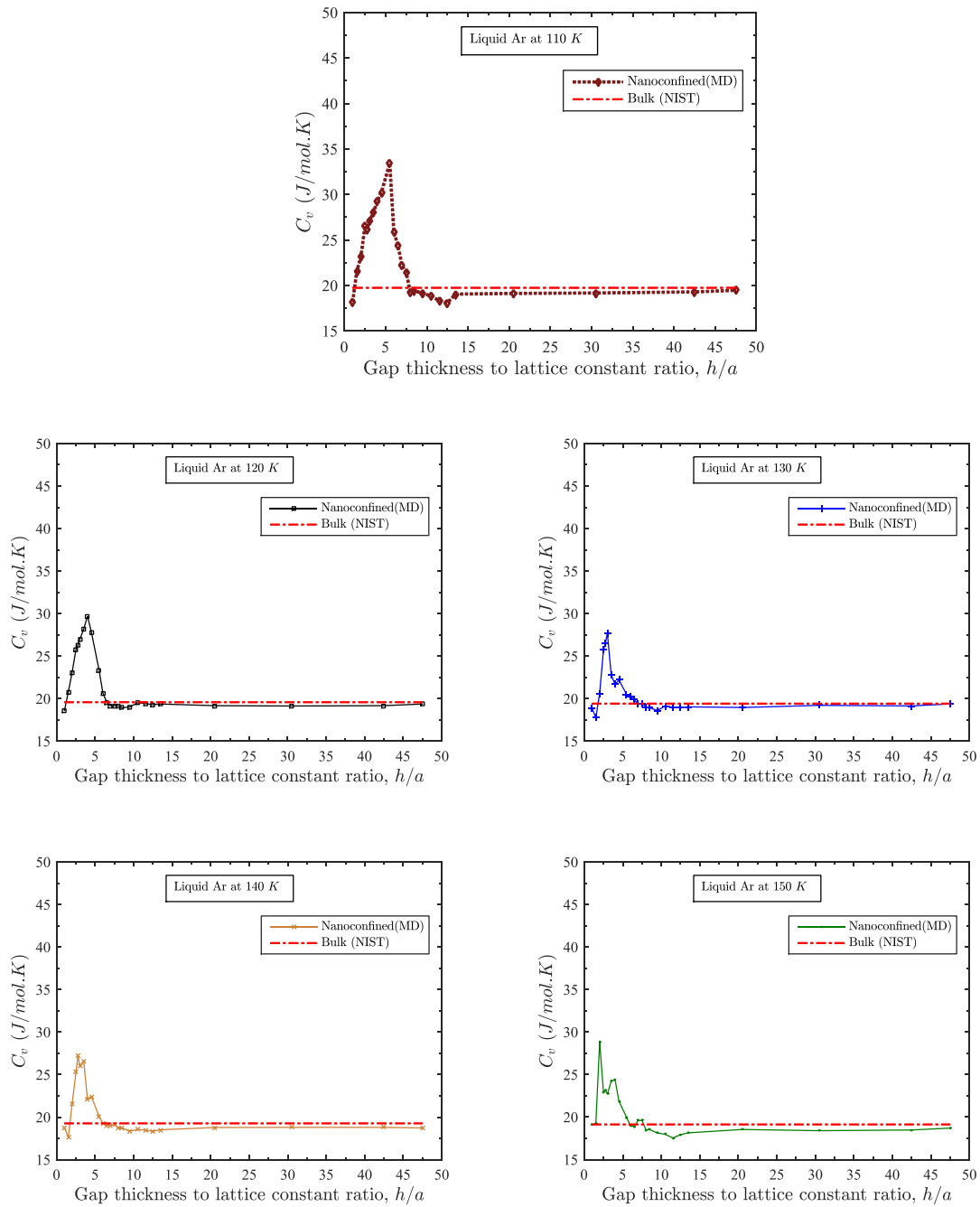


Figure 24: Variation of heat capacity with confinement height at different temperatures of the liquid. (a) for 110 K (b) for 120 K (c) for 130 K (d) for 140 K (e) for 150 K

The variation of heat capacity with gap thickness was extended for temperature variations (110K to 150K) as shown in Figure 24. In all the cases, a significant shift in heat capacity from the bulk value is observed but its magnitude strongly depends on temperature and gap thickness.

Figure 24 shows that the response of heat capacity of the confined liquid to the variation of gap thickness follows almost the same trend irrespective of the temperature of the confined liquid. Although the maximum value of heat capacity significantly varies. Moreover at higher temperature significant fluctuations in heat capacity is observed when the gap thickness approaches to its critical value from the bulk side. This is expected as higher temperature is associated with more energy of the confined liquid.
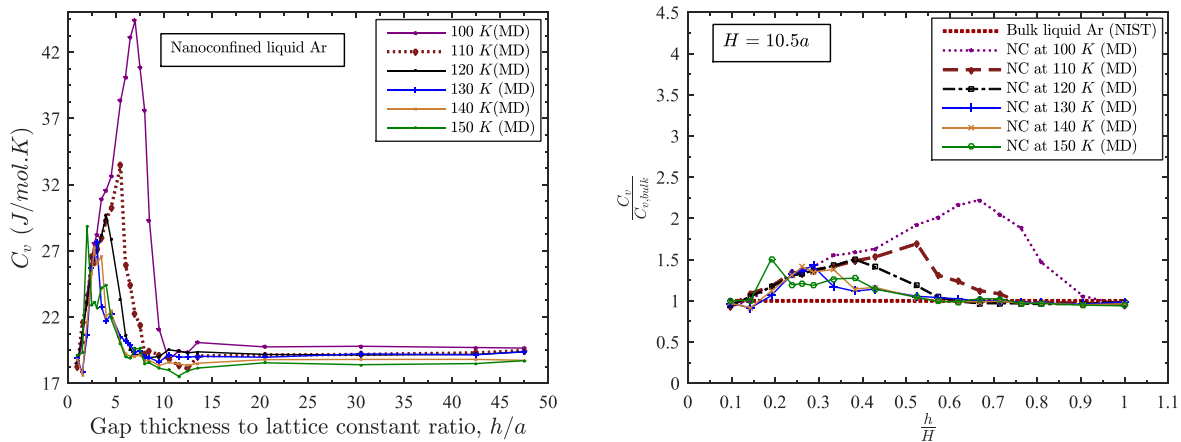


Figure 25: Combined effect of temperature and gap thickness on nanoconfined liquid (a) actual (b) normalized.

As seen from Figure 25 (a) variation of heat capacity occurs up-to h/a ~ 10.5, 8.0 and 6.0 for T=100 K, 110 K and 120 K respectively. For T= 130 K, 140 K and 150 K variation of $C_v$ is observed up-to h/a~5.5. The maximum value of heat capacity occurs at h/a ~ 7.0, 5.5, 4.0, 3.0, 3.5 and 2.0 for T=100 K to 150 K. The results indicate that the more the temperature of the confined liquid, the narrower the h/a band where significant fluctuation of heat capacity occurs and the lower the value of maximum heat capacity. But one thing that is common to all these three cases is that at h/a ~ 1.5, heat capacity of the confined liquid approaches to that of the bulk. These phenomena are pronouncedly visible in Figure 25 (b) where heat capacity is normalized by dividing it with the heat capacity of bulk liquid at that temperature and gap thickness is normalized by dividing it with h/a = 10.5. Another significant observation from Figure 25 is that although the band thickness

and the peak value of heat capacity is dependent on temperature, except for T=150 K case (which is nearest to the critical point of Ar, at that specified condition and hence can be justified), in rest of the cases, the slope of the increasing and decreasing portions of the curves are almost equal which depicts that the variation of heat capacity with respect to gap thickness is independent of temperature for nanogap confined liquid up to the corresponding critical value of h/a i.e. (h/a)*. The maximum value of heat capacity of the confined liquid decreases with the increase in temperature. As seen from Figure 25 (a) for temperature 100 K, the maximum heat capacity (44.7 J/mol. K) is around two times of the bulk liquid whereas for temperature 140 K, it's only around 1.2 times (27.1 J/mol. K). Previously many researchers have also reported the dependence of heat capacity on thickness and temperature for solid nanocrystals [16], [52].

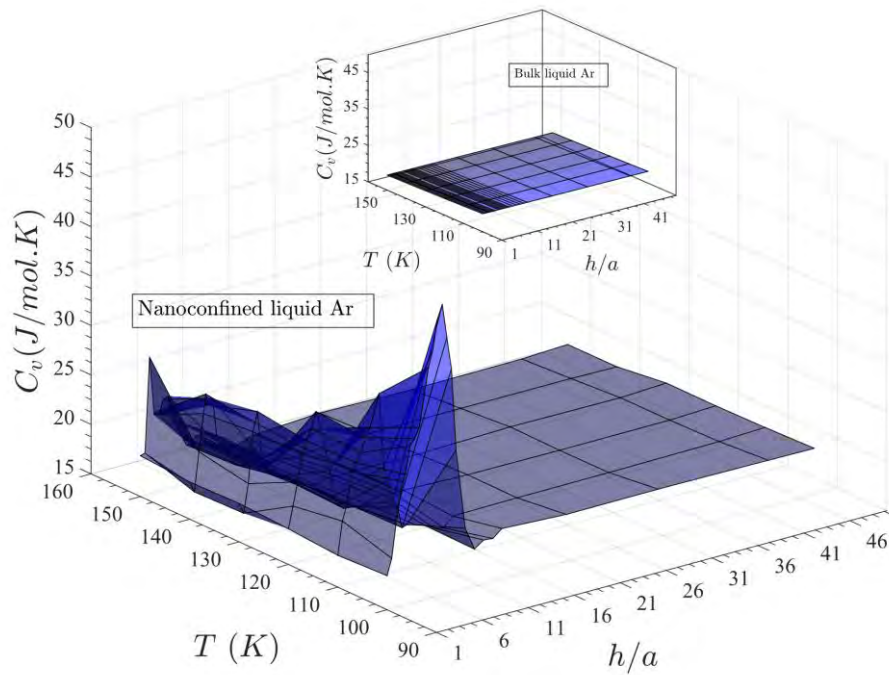## 7.3 RELATION AMONG GAP THICKNESS, TEMPERATURE AND HEAT CAPACITY



Figure 26: Heat capacity as a function of gap thickness and temperature.

In general, both the confinement gap thickness and temperature affect the heat capacity of confined liquid. The effect of confinement is valid up-to a certain range of gap thickness which directly depends on temperature. Within this thickness band, confinement enhances heat capacity. Beyond this band, heat capacity of the confined liquid resembles to that of the bulk. The effect of temperature is to decrease the heat capacity irrespective of gap thickness. But the sensitivity of this decrement highly depends on gap thickness. Beyond a certain range of gap thickness, the variation of heat capacity with respect to temperature is analogous to that of the bulk liquid. But within this range, its variation is more pronounced compared to the bulk. All these facts are depicted in Figure 26. The different response of heat capacity with the variation of temperature and gap thickness for bulk and nanoconfined liquid is clearly visible. From Figure 26, it is obvious that the variation of heat capacity occurs within a certain range of gap thickness and temperature as shown by the highlighted contour and the maximum heat capacity occurs for some specific values of temperature and gap thickness.

## 7.4 RELATION AMONG GAP THICKNESS, TEMPERATURE AND MAXIMUM HEAT CAPACITY
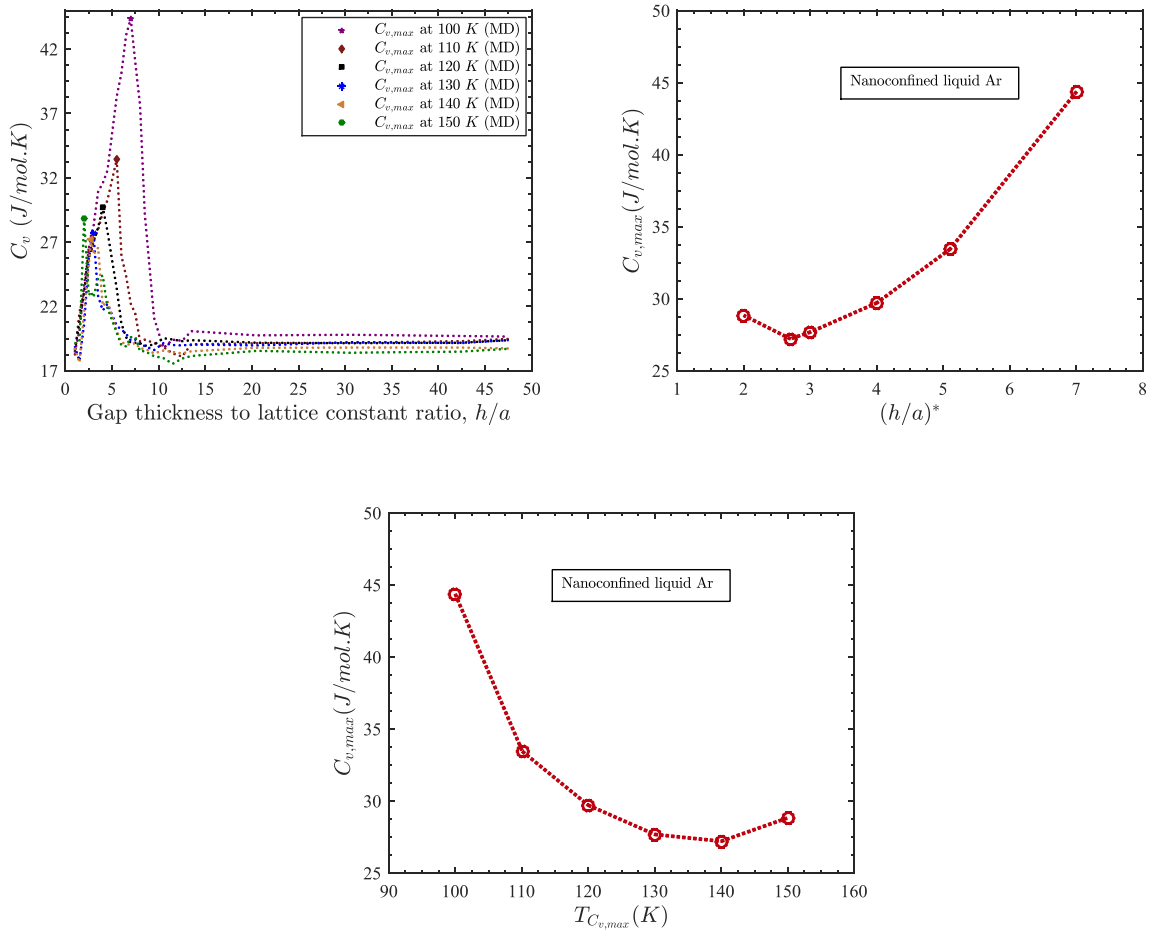


Figure 27: (a) Combined effect of temperature and gap thickness on nanoconfined liquid (Points of maximum heat capacity are highlighted) (b) Variation of maximum heat capacity with gap thickness (c) Variation of maximum heat capacity with temperature.

The maximum value of heat capacity is occasionally of great interest in many physical processes. Hence it is investigated separately in this section. The highlighted points as shown in Figure 27 (a) shows some indications that the decreasing values of maximum heat capacity with gap thickness and temperature follow some specific trends. This trend is pronounced in Figure 27 (b) and Figure 27 (c) where the maximum value of heat capacity is shown to vary with gap thickness and temperature separately. These graphs figure out that maximum value of heat capacity decreases if the confinement gap thickness and temperature – both are decreased or increased from some specified values.
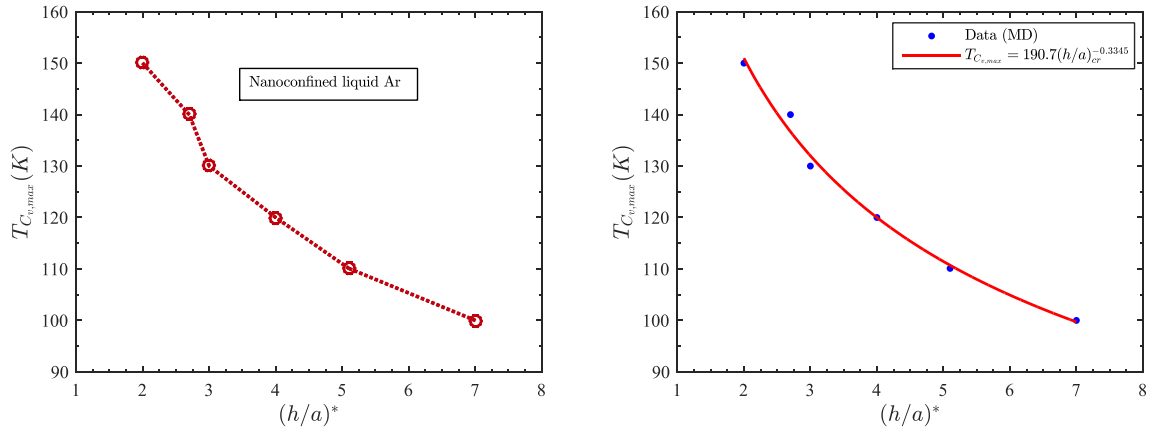
Figure 28: Relation between temperature and gap thickness for maximum heat capacity (a) Actual Curve (b) Best fit curve.

This one leads to an anticipation that the temperature and gap thickness at which maximum heat capacity occurs for a nanogap confined liquid are correlated. This one is shown in Figure 28 (a). From Figure 28 (b), it is found that the temperature at which maximum heat capacity occurs in the confinement varies with gap thickness following a power law, $T_{Cv,max} = 190.7 \left(\frac{h}{a}\right)^{-0.3345}$ although for bulk liquid, only temperature influences heat capacity and there is no influence of liquid film thickness on heat capacity of bulk liquid.
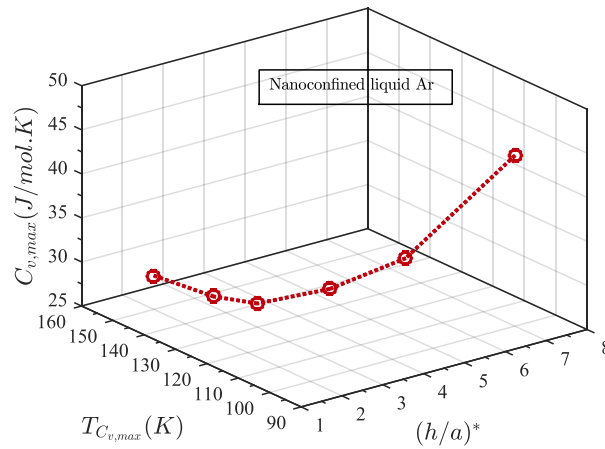


Figure 29: Combined effect of gap thickness and temperature for maximum heat capacity of nanogap confined liquid.

Figure 29 represents the maximum heat capacity of nanoconfined liquid Ar as a function of both the temperature and gap thickness. It indicates that maximum heat capacity occurs only at a specific configuration of the nanogap confined liquid i.e. only at some specific gap thickness and temperature of the confined liquid.

## 7.5 CONCLUSIONS

Non-equilibrium Molecular Dynamics (NEMD) simulations were employed in this section to investigate the combined effects of gap thickness and temperature on the heat capacity of nanoconfined liquid. It is found that for a specific range of gap thickness and temperature band, heat capacity of the confined liquid is higher than that of the bulk. Beyond that, it approaches to that of the bulk and this range is continuous, not discrete type. It also reveals that the maximum heat capacity occurs for a certain gap thickness and for a certain temperature of the confined liquid. Any alteration of this specified values reduces heat capacity from the maximum ones. This temperature and gap thickness are found to follow the power law, $T_{Cv,max} = 190.7 \left( \frac{h}{a} \right)^{-0.3345}$.

# CHAPTER 8

# CONCLUSION

Geometrically confined liquid behaves differently than the bulk one due to change of its configurational and vibrational states. Understanding the transport behavior of such fluid is of great importance for designing ultra-compact heat storage and heat flux devices. In this dissertation, with the aid of non-equilibrium classical molecular dynamics simulations and simplified solid-liquid molecular model, heat capacity of a nanogap confined liquid has been investigated. To explore how heat capacity of nanoconfined liquid responses with the variation of gap thickness and temperature were the main focus of this investigation. Key findings of the molecular simulations are:

- Nanoconfinement increases heat capacity of the liquid for a certain gap thickness and temperature range. Beyond that, heat capacity of the confined liquid approaches to that of the bulk liquid.
- For a certain temperature, increasing the gap thickness beyond one atomic layer increases the heat capacity; reaches a maximum value at some specified gap thickness and eventually decreases to align to that of the bulk value. This thickness band is strongly dependent on temperature.
- Like the bulk liquid, increasing the temperature decreases the heat capacity of the nanogap confined liquid irrespective of the liquid height. But this decrease in heat capacity with temperature may vary quite significantly than that of the bulk depending on the gap thickness.
- Maximum heat capacity, gap thickness and temperature-all are correlated. The temperature at which maximum heat capacity occurs for a nanoconfined liquid is observed to vary with gap thickness following the power law, $T_{Cv,max} = 190.7 \left(\frac{h}{a}\right)^{-0.3345}$
- Depending upon the temperature, for a particular gap thickness, the maximum heat capacity of the confined liquid can be more than double of the heat capacity of the bulk liquid.
- Changes in molecular configuration due to non-uniform density distributions, complex phonon transport mechanism, quantum effect, interfacial thermal resistance, mode of energy transfer – simultaneous effects of these variables are identified to cause this anomalous behavior.

# CHAPTER 9
# FUTURE RECOMMENDATION

Research presented in this dissertation has unveiled several parametric effects on heat capacity of the nanogap confined liquid. There are considerable scopes to extend the investigation for reaping further benefits from the nanoconfined liquid as outlined below:

a. Large-scale molecular dynamics can be used to evaluate the sensitivity of heat capacity to the structural and chemical disorder of the interface as well as with different surface wettability conditions like hydrophilic and hydrophobic ones.

b. Simulation with real molecules should be interesting and will provide more detailed information about the heat capacity of confined liquid.

c. Electronic contribution of liquid molecules in heat capacity will be a long-term goal to be conducted in atomic-level simulations.

d. Another important long-term challenge is the development of techniques that incorporate boundary scattering rates calculated by atomic-level simulations with higher-level approaches, e.g., Monte Carlo solutions of the classical or quantum Boltzmann transport equation.

# REFERENCES

[1] J. Israelachvili and D. Gourdon, "Putting liquids under molecular-scale confinement," *Science*, vol. 292, no. 5518, pp. 867–868, 2001.

[2] M. Alcoutlabi and G. B. McKenna, "Effects of confinement on material behaviour at the nanometre size scale," *J. Phys. Condens. Matter*, vol. 17, no. 15, pp. R461–R524, Apr. 2005.

[3] R. Devi, J. Sood, S. Srivastava, and K. Tankeshwar, "Diffusion of fluid confined to nanotube with rectangular cross section," *Microfluid. Nanofluidics*, vol. 9, no. 4–5, pp. 737–742, 2010.

[4] A. Shchepetov *et al.*, "Ultra-thin free-standing single crystalline silicon membranes with strain control," *Appl. Phys. Lett.*, vol. 102, no. 19, p. 192108, 2013.

[5] B. Bhushan, J. N. Israelachvili, and U. Landman, "Nanotribology: friction, wear and," *Nature*, vol. 374, p. 13, 1995.

[6] A. Maali and B. Bhushan, "Nanorheology and boundary slip in confined liquids using atomic force microscopy," *J. Phys. Condens. Matter*, vol. 20, no. 31, p. 315201, 2008.

[7] R. G. Horn and J. N. Israelachvili, "Direct measurement of structural forces between two surfaces in a nonpolar liquid," *J. Chem. Phys.*, vol. 75, no. 3, pp. 1400–1411, 1981.

[8] R. A. Donald, P. P. Pradeep, and D. Bhattacharya, "Essentials of materials science and engineering," *Thomson Publ.*, 2004.

[9] S. Maruyama and T. Kimura, "A study on thermal resistance over a solid-liquid interface by the molecular dynamics method," *Therm Sci Eng*, vol. 7, no. 1, pp. 63–68, 1999.

[10] X. Chen *et al.*, "Nanoscale fluid transport: size and rate effects," *Nano Lett.*, vol. 8, no. 9, pp. 2988–2992, 2008.

[11] Y. Tang, T. Fu, Y. Mao, Y. Zhang, and W. Yuan, "Molecule Dynamics Simulation of Heat Transfer Between Argon Flow and Parallel Copper Plates," *J. Nanotechnol. Eng. Med.*, vol. 5, no. 3, p. 34501, Aug. 2014.

[12] H. Zhang, H. Ye, Y. Zheng, and Z. Zhang, "Prediction of the viscosity of water confined in carbon nanotubes," *Microfluid. Nanofluidics*, vol. 10, no. 2, pp. 403–414, 2011.

[13] D. Ortiz-Young, H.-C. Chiu, S. Kim, K. Voïtchovsky, and E. Riedo, "The interplay between apparent viscosity and wettability in nanoconfined water," *Nat. Commun.*, vol. 4, Sep. 2013.

[14]    I. Avramov and M. Michailov, "Specific heat of nanocrystals," *J. Phys. Condens. Matter*, vol. 20, no. 29, p. 295224, Jul. 2008.

[15]    A. Rajabpour, F. Y. Akizi, M. M. Heyhat, and K. Gordiz, "Molecular dynamics simulation of the specific heat capacity of water-Cu nanofluids," *Int. Nano Lett.*, vol. 3, no. 1, pp. 1–6, 2013.

[16]    M. Michailov and I. Avramov, "Surface Energy, Surface Debye Temperature and Specific Heat of Nanocrystals," *J. Phys. Conf. Ser.*, vol. 398, p. 12008, Dec. 2012.

[17]    X. Hu, G. Wang, W. Wu, P. Jiang, and J. Zi, "The vibrational density of states and specific heat of Si nanocrystals," *J. Phys. Condens. Matter*, vol. 13, no. 39, p. L835, 2001.

[18]    Wikipedia, *Heat capacity — Wikipedia, The Free Encyclopedia*. 2017.

[19]    K. J. Laidler, *The World of Physical Chemistry*. Oxford, New York: Oxford University Press, 1995.

[20]    E. Wilhelm, T. Letcher, and R. S. of C. (Great Britain), *Heat Capacities: Liquids, Solutions and Vapours*. Royal Society of Chemistry, 2010.

[21]    P. Fraundorf, "Heat capacity in bits," *Am. J. Phys.*, vol. 71, no. 11, pp. 1142–1151, Nov. 2003.

[22]    J. Frenkel, "Kinetic Theory of Liquids,(1955)," *N. Y. Dover Publ*, vol. 8, p. 143.

[23]    D. Bolmatov, V. V. Brazhkin, and K. Trachenko, "The phonon theory of liquid thermodynamics," *Sci. Rep.*, vol. 2, May 2012.

[24]    J. Lee, J. Lim, and P. Yang, "Ballistic phonon transport in holey silicon," *Nano Lett.*, vol. 15, no. 5, pp. 3273–3279, 2015.

[25]    X. Li, "Phonon Transport across Dissimilar Material Interfaces and in Nanostructured Materials," 2012.

[26]    G. Chen, "Thermal conductivity and ballistic-phonon transport in the cross-plane direction of superlattices," *Phys. Rev. B*, vol. 57, no. 23, p. 14958, 1998.

[27]    Y. Wang, H. Huang, and X. Ruan, "Decomposition of coherent and incoherent phonon conduction in superlattices and random multilayers," *Phys. Rev. B*, vol. 90, no. 16, p. 165406, 2014.

[28]    J. Ravichandran *et al.*, "Crossover from incoherent to coherent phonon scattering in epitaxial oxide superlattices," *Nat. Mater.*, vol. 13, no. 2, pp. 168–172, 2014.

[29]    T. Yamamoto, S. Konabe, J. Shiomi, and S. Maruyama, "Crossover from ballistic to diffusive thermal transport in carbon nanotubes," *Appl. Phys. Express*, vol. 2, no. 9, p. 95003, 2009.

[30]   K. Takayanagi, Y. Kondo, and H. Ohnishi, "Suspended gold nanowires: ballistic transport of electrons," *JSAP Int.*, vol. 3, no. 8, 2001.

[31]   C. M. Hogan, "Density of States of an Insulating Ferromagnetic Alloy," *Phys. Rev.*, vol. 188, no. 2, pp. 870–874, Dec. 1969.

[32]   S. Sarkar and R. P. Selvam, "Molecular dynamics simulation of effective thermal conductivity and study of enhanced thermal transport mechanism in nanofluids," *J. Appl. Phys.*, vol. 102, no. 7, p. 74302, 2007.

[33]   D. Li, Y. Wu, P. Kim, L. Shi, P. Yang, and A. Majumdar, "Thermal conductivity of individual silicon nanowires," *Appl. Phys. Lett.*, vol. 83, no. 14, pp. 2934–2936, 2003.

[34]   C. Shao and H. Bao, "A molecular dynamics investigation of heat transfer across a disordered thin film," *Int. J. Heat Mass Transf.*, vol. 85, pp. 33–40, Jun. 2015.

[35]   A. K. M. M. Morshed, T. C. Paul, and J. A. Khan, "Atomistic simulation of temperature dependent thermal transport across nanoconfined liquid," *Phys. E Low-Dimens. Syst. Nanostructures*, vol. 47, pp. 246–251, Jan. 2013.

[36]   N. W. McNutt, Q. Wang, O. Rios, and D. J. Keffer, "Entropy-driven structure and dynamics in carbon nanocrystallites," *J. Nanoparticle Res.*, vol. 16, no. 4, Apr. 2014.

[37]   S. Merabia, S. Shenogin, L. Joly, P. Keblinski, and J.-L. Barrat, "Heat transfer from nanoparticles: A corresponding state analysis," *Proc. Natl. Acad. Sci.*, vol. 106, no. 36, pp. 15113–15118, 2009.

[38]   P. Hirunsit and P. B. Balbuena, "Effects of Confinement on Water Structure and Dynamics: A Molecular Simulation Study," *J. Phys. Chem. C*, vol. 111, no. 4, pp. 1709–1715, Feb. 2007.

[39]   K. Kurosaki, K. Yano, K. Yamada, M. Uno, and S. Yamanaka, "A molecular dynamics study of the heat capacity of uranium mononitride," *J. Alloys Compd.*, vol. 297, no. 1, pp. 1–4, 2000.

[40]   M. P. Allen and D. J. Tildesley, *Computer simulation of liquids*. Oxford [England] : New York: Clarendon Press ; Oxford University Press, 1987.

[41]   P. M. Agrawal, B. M. Rice, and D. L. Thompson, "Predicting trends in rate parameters for self-diffusion on FCC metal surfaces," *Surf. Sci.*, vol. 515, no. 1, pp. 21–35, 2002.

[42]   Q. Wang, D. J. Keffer, S. Petrovan, and J. B. Thomas, "Molecular Dynamics Simulation of Poly(ethylene terephthalate) Oligomers," *J. Phys. Chem. B*, vol. 114, no. 2, pp. 786–795, Jan. 2010.

[43]   R. B. Stewart and R. T. Jacobsen, "Thermodynamic properties of argon from the triple point to 1200 K with pressures to 1000 MPa," *J. Phys. Chem. Ref. Data*, vol. 18, no. 2, pp. 639–798, 1989.

[44]     "Thermophysical Properties." [Online]. Available: http://webbook.nist.gov/cgi/fluid.cgi?ID=C7440371&Action=Page. [Accessed: 11-Apr-2017].

[45]     D. Keffer, "The Working Man's Guide to Obtaining Self Diffusion Coefficients from Molecular Dynamics Simulations," *Dep. Chem. Eng. Univ. Tenn. Knoxv.*, 2001.

[46]     "Introduction to Physical Chemistry - Marcus Frederick Charles Ladd - Google Books." [Online]. Available: https://books.google.com.bd/books?id=juoR2_rnIuAC&pg=PA237&dq=mean+free+path+of +liquid+ar&hl=en&sa=X&redir_esc=y#v=onepage&q=mean%20free%20path%20of%20liq uid%20ar&f=false. [Accessed: 18-Jun-2017].

[47]     S. Plimpton, "Computational limits of classical molecular dynamics simulations," *Comput. Mater. Sci.*, vol. 4, no. 4, pp. 361–364, 1995.

[48]     A. Stukowski, "Visualization and analysis of atomistic simulation data with OVITO–the Open Visualization Tool," *Model. Simul. Mater. Sci. Eng.*, vol. 18, no. 1, p. 15012, 2009.

[49]     "NIST database." .

[50]     F. A. Gorelli, T. Bryk, M. Krisch, G. Ruocco, M. Santoro, and T. Scopigno, "Dynamics and Thermodynamics beyond the critical point," *Sci. Rep.*, vol. 3, Feb. 2013.

[51]     E. Tombari, G. Salvetti, C. Ferrari, and G. P. Johari, "Heat capacity of water in nanopores," *J. Chem. Phys.*, vol. 123, no. 21, p. 214706, 2005.

[52]     M. Barisik and A. Beskok, "Equilibrium molecular dynamics studies on nanoscale-confined fluids," *Microfluid. Nanofluidics*, vol. 11, no. 3, pp. 269–282, 2011.

[53]     G. Chen, *Nanoscale energy transport and conversion: a parallel treatment of electrons, molecules, phonons, and photons*. Oxford University Press, 2005.

[54]     E. S. Landry and A. J. McGaughey, "Effect of film thickness on the thermal resistance of confined semiconductor thin films," *J. Appl. Phys.*, vol. 107, no. 1, p. 13521, 2010.

[55]     Z. Liang and H.-L. Tsai, "Effect of molecular film thickness on thermal conduction across solid-film interfaces," *Phys. Rev. E*, vol. 83, no. 6, Jun. 2011.

[56]     A. M. Marconnet, M. Asheghi, and K. E. Goodson, "From the casimir limit to phononic crystals: 20 years of phonon transport studies using silicon-on-insulator technology," *J. Heat Transf.*, vol. 135, no. 6, p. 61601, 2013.

[57]     A. Joshi and A. Majumdar, "Transient ballistic and diffusive phonon heat transport in thin films," *J. Appl. Phys.*, vol. 74, no. 1, pp. 31–39, 1993.

[58]    P. K. Schelling, S. R. Phillpot, and P. Keblinski, "Comparison of atomic-level simulation methods for computing thermal conductivity," *Phys. Rev. B*, vol. 65, no. 14, p. 144306, 2002.

[59]    G. Balasubramanian, S. Banerjee, and I. K. Puri, "Unsteady nanoscale thermal transport across a solid-fluid interface," *J. Appl. Phys.*, vol. 104, no. 6, p. 64306, 2008.

[60]    E. Keshavarzi and M. Kamalvand, "Energy effects on the structure and thermodynamic properties of nanoconfined fluids (a density functional theory study)," *J. Phys. Chem. B*, vol. 113, no. 16, pp. 5493–5499, 2009.

[61]    L. Wang, Z. Tan, S. Meng, A. Druzhinina, R. A. Varushchenko, and G. Li, "Heat capacity enhancement and thermodynamic properties of nanostructured amorphous SiO 2," *J. Non-Cryst. Solids*, vol. 296, no. 1, pp. 139–142, 2001.

[62]    S. K. Roy, "Thermal Physics and Statistical Mechanics," p. 29,31.

[63]    K. S. Pitzer, *Molecular Structure and Statistical Thermodynamics: Selected Papers of Kenneth S Pitzer*. 1993.

[64]    E. T. Swartz and R. O. Pohl, "Thermal boundary resistance," *Rev. Mod. Phys.*, vol. 61, no. 3, p. 605, 1989.

[65]    A. K. M. M. Morshed, T. C. Paul, and J. A. Khan, "Effect of nanostructures on evaporation and explosive boiling of thin liquid films: a molecular dynamics study," *Appl. Phys. A*, vol. 105, no. 2, pp. 445–451, Nov. 2011.